CORE/CONCRETE INTERACTION EXPERIMENTS

D. POWERS

SANDIA NATIONAL LABORATORIES

December 1984

Item 1: BETA Tests

Response 1

These tests are quite similar to the COIL and CC tests([1]) sponsored by the U.S. Nuclear Regulatory Commission (USNRC) at Sandia National Laboratories (SNL) several years ago. The COIL and CC tests concentrated on sustained steel interactions with limestone concrete.

The BETA test are being done by the KfK in Germany. Early results of the BETA tests that have been made public include a motion picture or video tape showing the upper surface of the melt during sustained attack on concrete. Because an image can be seen without aerosols evident, it is often suggested that no aerosols were generated during the melt/concrete interaction. A question frequently posed is why are there no aerosols during this interaction yet aerosol production is clearly seen in analogous tests done in the COIL or CC tests as well as many other tests of core debris/concrete interactions done for the USNRC. Frequently, the clear implication made in posing the question is that there must be something "wrong" with the American tests or the methods currently used to estimate aerosol generation.

The question as posed is not easily answered. First of all, the BETA tests are of relatively recent origin. Very little data has yet been made available. Most important of these data would be quantitative evidence of the aerosol production (or the lack of it) in addition that which can be gleaned by inspecting a photograph record of the test. Secondly, modeling of the BETA tests might be possible were some essential data available. Among the data that are essential are melt temperatures and the composition of the concrete. Compositions of the concrete are needed in some detail since the most volatile constituents of concrete (such as sodium oxide and potassium oxide) are present at quite low levels. The volatile constitution of concrete is inadequately expressed by the term siliceous concrete or (and incorrectly for German concretes) basaltic concrete. Without these data a quantitative comparison of aerosol generation would be speculation.

On another front, the question addresses the larger issue of mechanisms involved in ex-vessel source term estimation done with the VANESA model. The primary mechanisms of aerosol formation considered in this model are:

(1) vaporization of species from the melt into the sparging gas.

(2) mechanical entrainment of melt droplets into the sparging gas.

70

Videotape records of the BETA tests suggest both mechanisms should be operative in these tests. What then might be the estimate of aerosol production during the tests obtained from the VANESA model?

The complication in obtaining an estimate of aerosol production posed by the current absence of melt composition data, concrete composition data and melt temperature data have been noted above. Another complication is that heat input to the melts involved in the BETA tests goes into the metallic phase. The overlying oxide layer is cooler and is heated by conduction and convection from the metallic phase. This is exactly opposte to a reactor accident case and violates an assumption in the VANESA model.

Ignore for the purposes here the complications above. Advice from investigators associated with the BETA tests is that melt temperatures are low - in the vicinity of the stainless steel liquidus. Assume here that this temperature is between 2000 and 1900K. Assume further that the concrete is made of basaltic aggregate (it is not, but this is an understood concrete). Then the VANESA model would predict an aerosol generation rate of 0.009 to 0.003 g/s. Typically, the aerosol so predicted is composed of:

Component	Percentage	Component	Percentage
FeO	0.5 w/o	Al_2O_3	0.02 w/o
Cr_{2O3}	0.01 w/o	Na_2O	5.3 w/o
Ni	0.09 w/o	K_2O	93 w/o
CaO	0.69 w/o	SiO_2	0.7 w/O

Of course, if any of the assumed inventories of melt constituents are in error, both the aerosol composition and the aerosol generation rate would be affected.

Quite clearly, as best as can be ascertained from the available data, VANESA predicts low aerosol generation rates for the BETA tests and low rates are apparently observed. This should add some credence to the validity of the VANESA procedure.

Item 2: Explain bubbling during core debris interactions with concrete.

Response 2

One of the first, most significant, observations made in USNRC-sponsored research on core-debris interactions with concrete was that gases bubbled up through the melt. It had been presumed at the time of the Reactor Safety Study that gases would pass around the melt because of the ferro-static head provided by the melt. Because gases bubble up through the melt, they can vigorously react with the melt. Thus unlike what was assumed in the Reactor Safety Study, vigorous ex-vessel production of flammable gases such as H_2 and CO is a prominant feature of seve e reactor accidents.

The gases produced during core debris attack on concrete are H_2O and CO_2 generated by pyrolysis of concrete constituents. The release of these gases

affects thermal transport in the concrete and the ability of heat to be transported from the core debris to the concrete. Macroscopic data have shown for instance that heat to the concrete is reduced by a factor of five between siliceous and limestone concrete as a result of higher gas generation rates in the case of limestone concrete([2]). Further, the gases provide a vastly increased surface area for the vaporization of modestly volatile species from the melt. These volatile species, once cooled after escaping the melt, form aerosols.

Needless to say, details of gas behavior have been of intense interest for modeling core debris interactions with concrete. In response to this interest, research programs sponsored by the USNRC have taken several steps to provide more detailed data:

(1) Melts after solidification have been sectioned to ascertain if useful information can be derived from trapped structures.

(2) Acoustic studies during melt/concrete interactions have been conducted.

(3) The attack of melts on concrete have been monitored by x-ray and gamma ray image intensification to show in real time the behavior of the melt and gas bubbling.

Sectioning of melts has had mixed utility. In some cases bubbles have indeed been trapped in the frozen melt. These bubbles are ellipsoids with a long dimension of between 1 and 2 cm.([2]). In other cases, no bubbles have been trapped in the solidified melts([1]).

Acoustic studies of melt/concrete interactions were conducted by reflecting a sonic wave off the melt/concrete interface([3],[4],[5]). These studies yielded data that was not uniquely interpretable. On the one hand, phase inversions were observed that were indicative of a continuous interfacial gas film. On the other hand, intermittent "noise" in the signals was indicative of isolated bubble formation. (Incidently, the acoustic monitoring technology was given to KfK.)

The most useful technique for examination of bubble behavior was the x-ray image intensification([6]). Tests monitored by x-ray show isolated bubbles seemingly formed at preferred locations that may be the result of Taylor instabilities. Heat fluxes to the concrete are high in these regions of preferred bubble generations. The bubbles are so-called "wobbly ellipsoids"([7]) with maximum dimensions of 1-2 cm. Inspection of bubble shapes superimposed over plots of Eotvos, Reynolds, and Morton numbers (see Figure 1) shows that only modest changes in melt properties can cause bubbles to vary between wobbly ellipsoids and spherical caps.

Results of the studies of bubble formation during core debris attack on concrete seem entirely consistent with bubbling during so-called oxygen "blows" during steel making by the basic oxygen furnace (BOF) method. During BOF steelmaking, pig iron is decarburized by directing an oxygen stream at the melt surface. Carbon monoxide bubble nucleate in pores of the refractory material used to confine the melt. These bubbles are typically 1-2 cm in diameter and

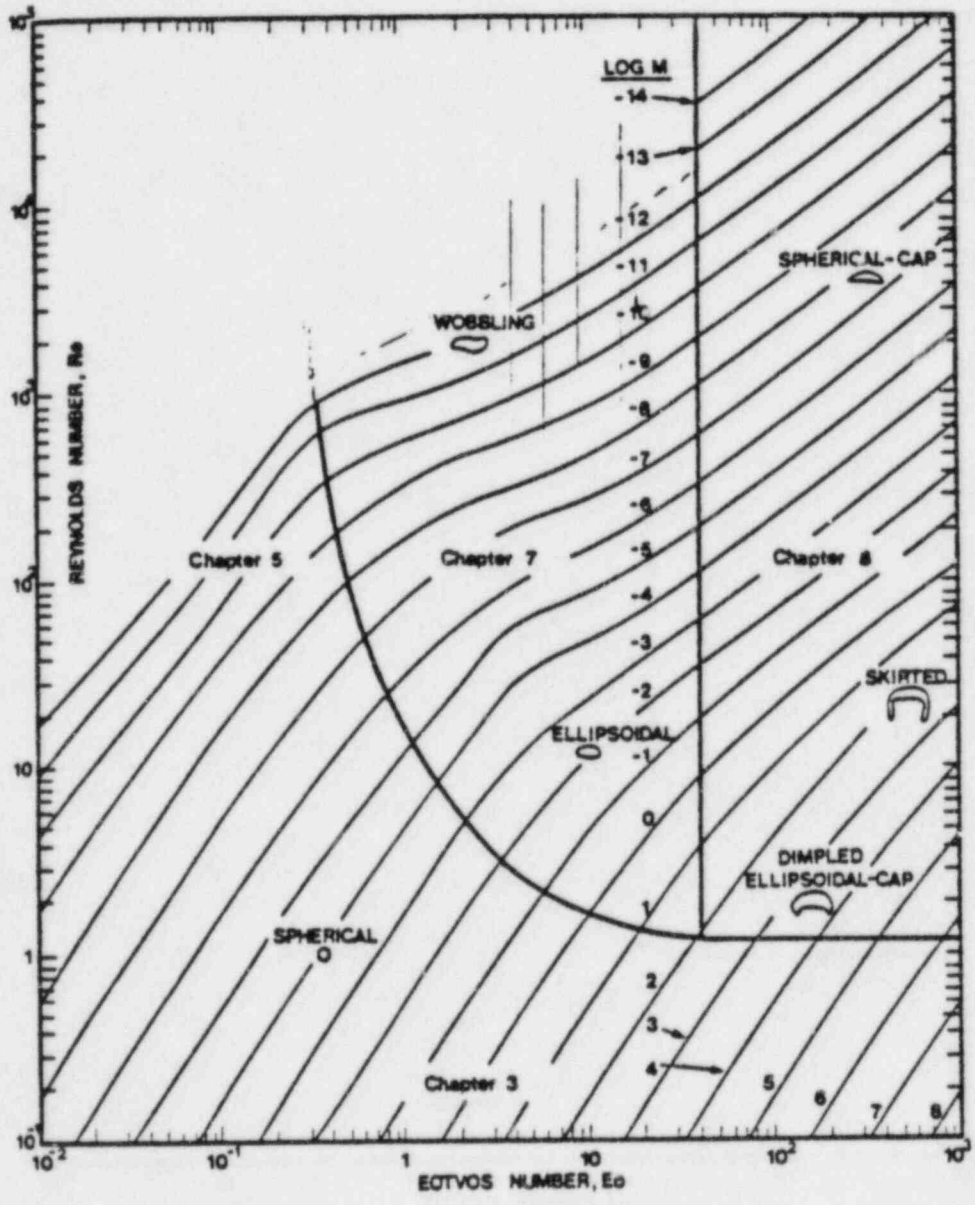

Fig. 1 Shape regimes for bubbles and drops in unhindered gravitational motion through liquids.

have usually been characterized as spherical caps. During the "blow," several tons of a 100-200 ton mass are lost. The lost mass is carbon and volatile constituents of the melt such as Mn and Fe. The broad data base on oxygen "blows" was used extensively in the development of the VANESA model.

Item 3: Explain layering in light of bubbling.

Response 3

Another, early, important observation of the experimental studies of core debris interactions with concrete sponsored at SNL by the USNRC was that melts stratified according to density into oxide and metal phases. The hypothesis used in developing the Reactor Safety Study model was that the melt was thoroughly homogenized (the so-called "homogeneously heterogeneous" approximation.) Stratification was repeatedly observed in a variety of tests and is, again, consistent with the experience in the steel industry. Stratification is not perfect. An interfacial regime has been found after sectioning some melts([2]) that suggests some intermingling of phases near the interface. This zone is typically no more than 2-3 centimeters deep.

Many scientists upon viewing films of melt/concrete interactions and the violent melt agitation by sparging gases, are not persuaded of stratification. Fortunately, the stratification has also been clearly visible in tests monitored by image intensification. There seems no doubt then that stratification of the melt into layers is not undone by the effects of gas generation.

Another source of confusion concerning stratification has been created by the recent BETA tests of steel/concrete interactions. These tests use a long, narrow concrete crucible. I. Catton[8] seems to have been the first to note that frozen material composed of both oxidic and metallic phases may be a unique feature of the extreme aspect ratio of the crucible. He suggests that gases generated at the walls and the base of the crucible cause the melt to "chug". Material from the mixed zone between the oxide and the metal layers freezes on the cooler concrete walls during chugging. The frozen material does not couple effectively with the inductive heat source because the metal phase is a distributed particulate. Consequently, as the test progresses, more and more material freezes on the walls. Post-test, it can appear that there was rather vigorous mixing of the melt and oxide. Professor Catton's suggestion would explain why declining power inputs are consistently observed over the course of the BETA tests.

Wall effects and the like have been observed in NRC-sponsored tests even at aspect ratios (height-to-diameter) of one. For this reason the NRC-sponsored research has gravitated toward the use of concrete crucibles in which only the base is concrete and the walls are an inert refractory material.

Stratification of the melt has been observed mostly in tests which used a simulant as the oxide phase. The New Small Scale (NSS) tests done at SNL, which involved prototypic corium melts, also demonstrated stratification. In these tests, three layers were observed. At the bottom of the crucible was a dense oxide layer composed primarily of UO_2 and ZrO_2. At the top of the crucible was a light oxide layer composed primarily of molten concrete. Between the two oxide layers was a stainless steel layer.

It is upon the basis of observations from the x-ray monitored tests and the results of the NSS tests that the layer structure was devised for CORCON. The model allows distinct layers with or without a mixed interfacial region. The interfacial region, at the option of the user can be extended to include the entire melt volume so that, in effect, one has a well-mixed melt. Options for interfacial mixing are seldom invoked simply because there are insufficient data to defend a description of the interfacial zone.

The relative orientation of layers is continuously interrogated in the course of CORCON calculations. Calculations are usually initiated with the fuel oxide phase more dense than the metal. As concrete ablates, condensed products of concrete decomposition are incorporated into the oxidic melt reducing its density. Eventually, the oxide layer becomes less dense than the metal layer and the two layers reverse positions (layer flip). This is modeled as an instantaneous position exchange. Obviously this is not correct. Rather than a sudden "flip" there will be a period during which the oxide and metal phases have very similar densities. During this transient period agitation by gas bubbles would be sufficient to cause the melts to mix and be a "homogeneously heterogeneous" mixture. As concrete ablation continues the oxide phase becomes even less dense. Test data show that stable stratification would be re-established.

Two issues of current concern to those developing models of core debris/concrete interactions are:

(1) is the oxide phase of a core melt initially more dense than the metal phase?

(2) how extensive is metal entrainment into the oxide phase as a result of gas bubbling?

Modeling in CORCON and most conventional density analyses suggest indeed that the oxide phase of a core melt is more dense than the metal phase initially. Recent analyses of condensed phase equilibria suggest that this may not always be true. The analyses also show that the procedure used in the WECHSL code to enforce the metal to be more dense than the oxide may be in error in some cases. This is an area of ongoing research.

Laboratory research with simulants has suggested that gas bubbling will cause significant entrainment of metallic melt into an overlying oxidic melt phase. This entrainment vastly increases the heat transfer between the oxide and metal phase. One of the important differences between CORCON mod 2 and earlier versions of CORCON is a heat transfer coefficient for interfacing melt layers that recognizes the enhancement caused by entraining.

Entrainment has recently been critized.([9]) The arguments opposing entrainment are that while it is observed with simulants, it will not occur with prototypic melts. Empirical evidence suggests that when entrainment is included, predicted melt temperatures are too low. Both the empirical evidence and the entrainment arguments have been criticized. Again, this must be considered an area of ongoing research.

Item 4: The TURC Tests.

Response 4

It is recognized that the descriptions of ex-vessel core debris interactions have been based on experimental data derived from steel melts. Steel constitutes but a portion of the core melt. Perhaps the more important portion of a core melt is the oxidic phase. In response to this concern SNL has developed the technology to prepare large-scale (>200 kg) melts of UO_2-ZrO_2 or more complex mixtures of UO_2 - ZrO_2 - Zr. Those experiments, called the TURC tests, have been the first tests to utilize this technology to investigate core debris interactions with concrete.

A series of 4 TURC tests were run. The objective of the tests was to determine if there were significant differences between the behavior of metallic melts and the behavior of oxidic melts during attack on concrete. The test series was then formulated to begin with two metallic melt/concrete interaction tests. Metallic melts were prepared by metallothermic and by furnace methods. These two tests, TURC 1T and TURC 1SS, constituted a touchstone to the vast array of metal melt/concrete interaction studies. The third test, TURC 2, used a melt of UO_2 - 25w/o ZrO_2. The last test in the TURC series, TURC 3, used a melt of UO_2 - 25w/o ZrO_2 - 10w/o Zr. Test TURC 2 and TURC 3 are the only large-scale urania melt/concrete interaction tests.

The TURC tests have only recently been completed and both reduction and analysis of the data from the tests are still underway. Some preliminary conclusions are:

(1) There are substantive differences in the behavior of oxidic melts and metallic melts during attack on concrete.

(2) The gas-film model used in CORCON and WECHSL to model heat transfer from the core debris to concrete cannot be universally correct.

(3) Interfacial crusting is insignificant for metals attacking concrete but is of dominant influence for oxidic melts attacking concrete.

(4) Relief of interfacial crusting by incorporation of ablated concrete is simulated too rapidly by CORCON mod 2.

(5) All CORCON mods predicted well the test behavior in TURC 1T which used a Thermitically generated melt. The CORCON mods underpredicted concrete erosion in the test with a furnace-prepared stainless steel melt and overpredicted erosion with an oxidic melt.

Melts used in the TURC tests were doped with elements that would be radioactive in a real reactor accident. The tests were extensively instrumented for aerosol production. Again, only limited results of the aerosol measurement are available at this time. Among these early results are:

(1) Geometrical data on the evolved aerosol are consistent with VANESA predictions.

(2) Tellurium release was extensive in all tests as would be predicted with the VANESA model

(3) Molybdenum release was extensive and this would not be predicted by VANESA.

Enough aerosol size data have been collected that the developers of the VANESA model are confident of the model's size predictions. The TURC tests seem to enforce this confidence.

Aerosols evolved during the TURC tests contained substantial amounts of molybdenum. Extensve Mo release was also observed in the smaller NSS tests that used corium melts. Unfortunately, the VANESA model predicts negligible Mo releases. As yet there is only speculation over the causes of the erroneous predictions.

The TURC tests provide valuable data that will greatly assist in the refinement of the models of ex-vessel core debris interactions. The TURC tests presage a second test series, the SURC tests. In the SURC tests, currently planned to be a series of 6 tests, uranium dioxide melts will be sustained while in contact with concrete. The SURC test will begin in the spring of 1985 and continue through October.

Item 5: The SWISS (Sustained Water Interaction with Stainless Steel) Tests.

Response 5

Many hypothesized severe reactor accidents involve not core debris/concrete interactions but combined core debris/concrete/coolant interactions. The SWISS tests were done at SNL to examine the effects of coolant on core debris/concrete attack. The tests are somewhat similar to though smaller than the BETA tests and the COIL tests. A 45 kg metallic melt is prepared to a known temperature. It is then deposited into a concrete crucible and sustained with induction heating. After a period of 1-20 minutes water flows over the melt at a rate of 11 gallons/minute. Two SWISS tests were done in September. A third will be done this winter.

Primary results obtained from the SWISS tests are:

(1) Addition of water did not alter attack on the concrete by the molten steel.

(2) Addition of water inhibited but did not halt aerosol production.

The first of these results casts doubts on scenarios in some probabilistic risk assessments in which it is assumed that injected water will ipso facto quench, fragment and halt attack on concrete. To date, authors of these probabilistic studies have chosen to cling to their hypotheses which are unsupported by data and to ignore results of the SWISS test calling them "too small".

The second of the SWISS test results confirms a prediction by VANESA that overlying water pools mitigate ex-vessel release. The confirmation, is however, only qualitative. The SWISS tests suggest that the VANESA model may underpredict the extent of mitigation by as much as a factor of 10. The SWISS results

also show that models of ex-vessel release based on surface temperatures such as that developed by IDCOR cannot be correct because the release was observed even after surfaces were cooled to water saturation temperatures.

Techniques developed in the SWISS test series will be applied to the SURC tests described above. In some of the SURC tests water addition during melt/concrete interaction will be examined.

Item 6: Measurements of Lanthanum Oxide Vapor Pressure

Response 6

Lanthanum oxide is assumed to vaporize into the gaseous species La(g), LaO(g), LaOH(g) and $La(OH)_2(g)$. Thermochemical data used in the VANESA calculations were all taken from secondary sources. Data for La(g) were from the compendium:

Hultgren, Orr, Anderson and Kelly, Selected Values of Thermodynamic Properties of Metals and Alloys, J. Wiley and Sons

Data for the other lanthanum species were from the compendium:

D. D. Jackson,
UCRL-51137 Lawrence Livermore Laboratory
Livermore, CA., 1971

Recently, an improved collection of data for monoxide vapor species has appeared:

J. B. Pedlegand and E. M. Marshall, "Thermochemical Data for Gaseous Monoxides," J. Phys. Chem. Ref. Data, 12 (1983) 967.

The VANESA model has not yet been revised to include these more recent recommendations.

Primary data sources abound for the species LaO(g). Free-energy functions for gaseous species are nearly always derived from spectroscopic data. Some sources are as old as 1928 and as recent as 1974. Dissociation energies and the like are nearly always taken from Knudsen effusion and mass spectroscopic work. The most recent review of data for LaO(g) recommends the primary source:

R. J. Ackermann and E. G. Rank, J. Chem. Thermodynamics, 3 (1971) 445.

Item 7: Describe how Pu is represented in VANESA.

Response 7

Plutonium is not explicitly treated in VANESA. Rather, the vaporization is assumed to be adequately represented by the vaporization of CeO_2. Cerium dioxide is assumed to have vaporized into the gaseous species Ce(g), CeO(g), Ce OH(g) and $Ce(OH)_2(g)$. Both cerium and plutonium form a vapor phase dioxide which is, like many other gaseous species, neglected in the VANESA model. Results obtained with VANESA are then lower bounds on the true vaporization since some gaseous species are neglected.

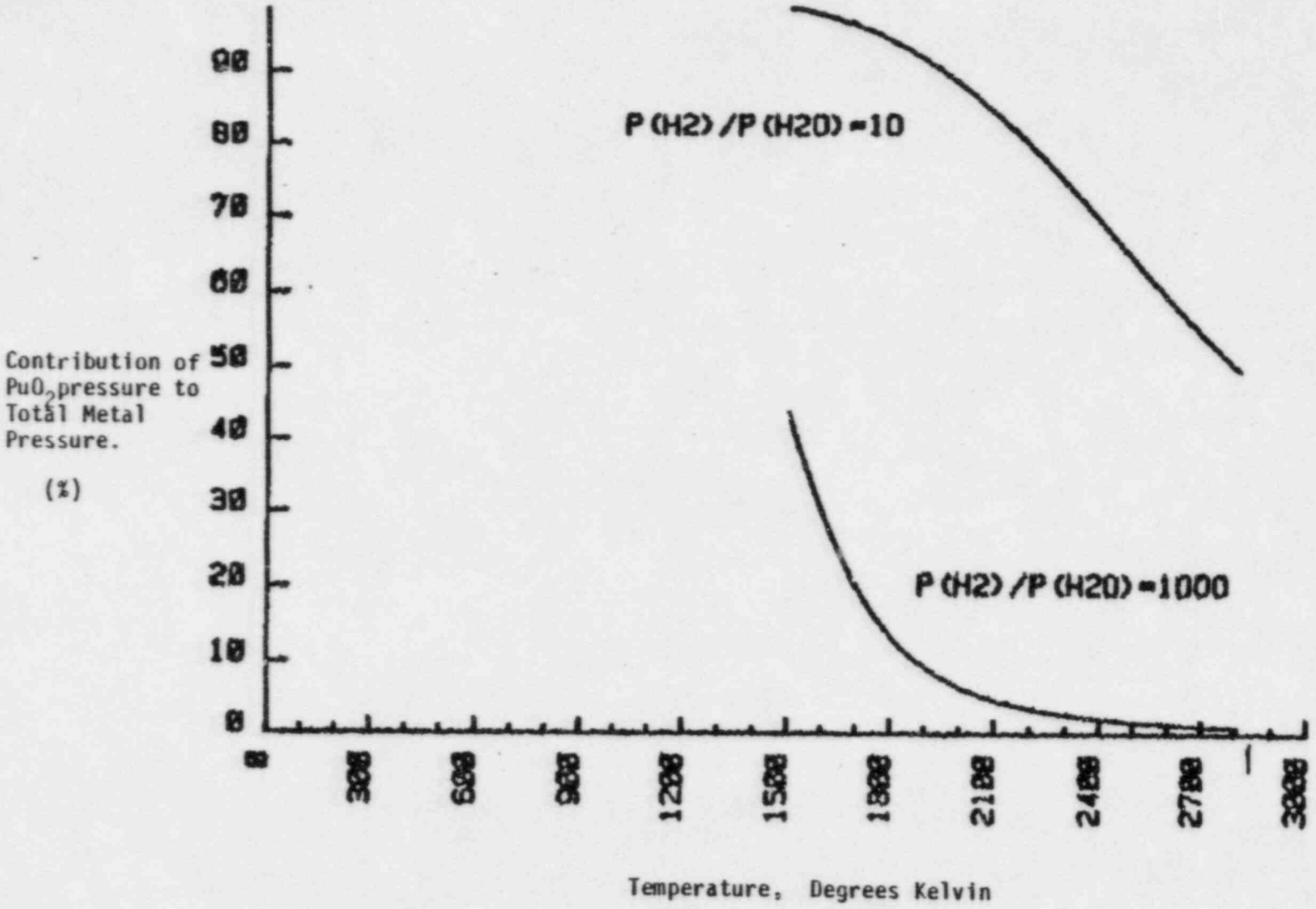
Contribution of PuO_2 pressure to Total Metal Pressure.
(%)
90
80
70
60
50
40
30
20
10
0
P (H2) /P (H2O) =10
P (H2) /P (H2O) =1000
Temperature, Degrees Kelvin

The importance of $PuO_2(g)$ can be quantified. A plot of the contribution of $PuO_2(g)$ to the metal-bearing gas Pu(g), PuO(g), and $PuO_2(g)$ is shown in the enclosed figure. $PuO_2(g)$ is quite important when the P_{H_2}/P_{H_2O} ratio is low (or equivalently the oxygen potential is high). However, when this ratio is low, so too is the absolute pressure of plutonium-bearing gas. $PuO_2(g)$ makes little contribution to the vapor for high ratios of P_{H_2} to P_{H_2O}. This ratio is, of course, quite higher when Zr is present in the melt. That is, when Zr is present, the release of the refractory species is important.

Both PUO_2 and CeO_2 can be nonstrichsometric. That is, they can have actual compositions PuO_{2-x} and CeO_{2-x} where x is a function of the oxygen potential. This non-strichsometry form is neglected in VANESA. The neglect of nonstrichsometry does not appreciably affect the vapor pressures as shown in the enclosed figure.

Item 8: Discuss the relative volatility of La_2O_3 and UO_2

Response 8

Vaporization processes involving constituents of the melt may be described by reactions such as:

Uranium

$$UO_2 + H_2 \rightarrow UO(g) + H_2O$$

$$UO_2 + 2H_2 \rightarrow U(g) + 2H_2O$$

$$UO_2 + H_2O \rightarrow UO_3(g) + H_2$$

$$UO_2 + 2H_2O \rightarrow UO_2(OH)_2\ (g) + H_2$$

$$UO_2 + H_2 \rightarrow U(OH)_2\ (g)$$

$$UO_2 + 3/2H_2 \rightarrow UOH(g) + H_2O$$

$$UO_2(c) \rightarrow UO_2(g)$$

Lanthanum

$$La_2O_3 + H_2 \rightarrow 2\ LaO(g) + H_2O$$

$$La_2O_3 + 3H_2 \rightarrow 2\ La(g) + 3H_2O$$

$$La_2O_3 + H_2 \rightarrow La_2O_2(g) + H_2O$$

$$La_2O_3 + H_2O + H_2 \rightarrow 2\ La\ (OH)_2(g)$$

$$La_2O_3 + 2H_2 \rightarrow 2\ LaOH(g) + H_2O$$

The vaporization of the urania and the lanthanides is proportional to the sum of the equilibrium partial pressures of the vapor species. The thermochemical

definition of the equilibrium partial pressure of a species can be written in the general case as:

$$-\Delta G^{(i)}_{RXN}(T)/RT = a \ln P_{H_2} + b \ln P_{H_2O} - \ln a_{MO} + u \ln P_i$$

where $\Delta G^{(i)}_{RXN}(T)$ = standard state free-energy change associated with the ith reaction going to the right as written above at temperature T

P_{H_2} = equilibrium hydrogen partial pressure.

P_{H_2O} = equilibrium partial pressure of H_2O.

P_i = equilibrium partial pressure of the ith vapor species.

R = gas constant.

a, b = coefficients dependent on the reaction stoichiometry and may be greater than, less than or equal to zero.

u = coefficient dependent on the stoichiometry of the reaction and for reactions written as above is greater than zero.

a_{MO} = activity of the parent oxide (UO_2 or La_2O_3) in the melt.

For instance, for the reaction

$$La_2O_3 + H_2 \rightarrow 2\,LaO(g) + H_2O$$

$$-[2\Delta G_f(LaO(g)) + \Delta G_f(H_2O) - \Delta G_f(La_2O_3)]/RT = -\Delta G_{RXN}/RT$$

$$= -\ln P_{H_2} + \ln P_{H_2O} - \ln a_{La_2O_3} + 2 \ln P_{LaO}$$

The activity of the parent species in the melt is by definition just the mole fraction multiplied by an activity coefficient. An approximation that increases in accuracy with increasing temperature is to assume the activity coefficient is one (ideal solution approximation). Then,

$$\text{Vaporization rate} \propto \sum_{i=1}^{N} P_i \propto a_{MO} \propto X_{MO}$$

where X_{MO} is the mole fraction of the parent, condensed species and the symbol $\propto$ denotes "proportional to." Thus, for two species, I and J with identical chemistry, the ratio of their vaporization rates would be:

$$\frac{V_R(I)}{V_R(J)} \propto \frac{(X_I)^{1/u_I}}{(X_J)^{1/u_J}}$$

where $V_R(K)$ is the vaporization rate of the $K^{\underline{th}}$ melt constituent.

Comparing the relative concentrations of La_2O_3 and UO_2 in the SURRY TMLB' melt and assuming La_2O_3 and UO_2 have identical chemistry would suggest the following:

$$\frac{V_R(La_2O_3)}{V_R(UO_2)} \sim 10^{-3}$$

But, La_2O_3 and UO_2 do not have identical chemistries. Inspection of possible vaporization reactions of La_2O_3 show these reactions are promoted by reducing conditions. That is, trivalent lanthanum in the melt vaporizes to form divalent lanthanum in the gas. Vaporization of lanthanum can also yield monovalent and atomic species. Vaporization of urania on the other hand can be promoted by both oxidizing and reducing conditions. Under reducing conditions tetravalent urania will vaporize to form divalent, monovalent and atomic species. Under oxidizing (in this case steam-rich) conditions, tetravalent urania can vaporize to form hexavalent species such as $UO_3(g)$ and $UO_2(OH)_2(g)$.

Whether conditions are oxidizing or reducing depends of course on the species in question. For both La_2O_3 and UO_2, conditions produced when H_2O and CO_2 from the concrete sparge through a melt of Zr and stainless steel are reducing. The steam and carbon dioxide are reduced extensively to hydrogen, carbon monoxide and even carbon. Thus, early in the SURRY TMLB' accident when there is some Zr present in the metallic core debris, vaporization of both lanthanides and urania should be efficient. The concentration effect described above suggests as a rough approximation that lanthanides and urania ought to vaporize in a ratio of about 1:1000.

Eventually, during the course of the ex-vessel phase of the accident, all the zirconium in the metallic portion of the core debris is converted to ZrO_2 by reaction of the gases from concrete. Once the zirconium has been consumed and any carbon in the melt has been consumed the gases from the concrete react with the mixture of Fe, Cr and Ni to form H_2 and CO. Reaction with the Fe, Cr, and Ni mixture is not nearly as complete as reaction of gases with a zirconium-bearing melt. Thus, relative to urania and lanthanum oxide, conditions in the melt are mildly oxidizing despite the fact the ratio of hydrogen and steam partial pressures is on the order of 3-5. Under these conditions lanthanum oxide vaporization is inhibited both in the absolute sense and relative to urania. The precise quantification of vaporization and its dependence on prevailing conditions is, of course, what is done in the VANESA model.

The preceeding discussion was, of course, directed toward the lanthanum/urania relative vaporization. Analogous arguments can be formulated for cerium oxide vaporization and alkaline earth vaporization. The discussion of ruthenium and molybdenum vaporization take on a somewhat different tone since these elements vaporize from the metal phase.

Item 9: Contrast Releases of Lanthanum and Uranium for Accidents at Surry and Peach Bottom

Response 9

All plants and all accidents are different so to respond effectively one needs to focus on specific accidents. Here concentrate on the Surry TMLB' and the Peach Bottom AE accidents. The essential point of creating the VANESA model is that a computational tool is needed that is responsive to the unique features of both the plants and the accidents. The two accidents listed above will illustrate the sensitivity of VANESA to both accident and plant conditions. The two accidents have almost nothing in common. In Table 2 are listed some of the differences between the two accidents. Parameters that make a difference for release are:

(1) Concentration of volatiles in melt.

(2) Melt temperature.

(3) Gas flow rates.

(4) Oxygen potential of the melt.

Consider just the concrete in the two reactors. Surry has a siliceous concrete with a low ablation temperature and a low heat of ablation. Peach Bottom has a limestone concrete which ablates at quite a high temperature; great amounts of heat must be expended to decompose carbonates in the concrete and raise the condensed products of decomposition to the ablation temperature. Consequently, for a given amount of heat imparted to Surry concrete, more decomposition products are incorporated into the melt and less gas is liberated than in the Peach Bottom concrete. Dilution of the melt with ablated concrete reduces the volatile fission product concentration and consequently the volatility of the fission products; it also cools the melt and makes it more difficult to raise the melt temperature.

From the very start of core debris concrete interactions, the core debris covers more surface area of the Surry reactor cavity than the Peach Bottom reactor cavity. Since upward heat losses are proportional to surface area, the Surry melt will try to cool more rapidly at a given temperature than will the melt at Peach Bottom.

There is far more Zr initially present in the melt at Peach Bottom than in the melt at Surry. Combustion of Zr in the core melt by reaction with H_2O and CO_2 from the concrete provides a heat source that adds to the heating of core debris beyond what is available from radioactive decay heating. Zr also assures that gases passing through the melt will be reducing; this condition favors the vaporization of oxides often considered refractory such as CeO_2, La_2O_3 and SrO. It would then be expected that releases should be greater for Peach Bottom than for Surry.

A somewhat subtle point arises in connection with Zr reactions with CO_2. Reduction of CO_2 by Zr can go completely to carbon:

$$[Zr]_{melt} + CO_2 \rightarrow ZrO_2 + [C]_{melt}$$

where the symbol $[\ ]_{melt}$ indicates that the bracketed species is dissolved in the metallic melt. Once the Zr inventory is depleted carbon is the most reducing species in the metallic melt. Consequently reactions such as these become possible:

$$[C]_{melt} + H_2O \rightarrow CO + H_2 \qquad [C]_{melt} + CO_2 \rightarrow 2CO$$

When one mole of gas enters the melt, two moles of gas emerge during reaction with dissolved carbon. This means that for a period in the interaction of a zirconium rich melt with limestone concrete, there will be intense gas evolution. Not only does the gas carry heat from the melt, but also the chemical reaction responsible for the additional gas generation is endothermic. There are then powerful cooling mechanisms operative for core debris/concrete interactions in the Peach Bottom accident. Because the initial Zr inventory is smaller and the CO_2 content of the concrete is less at the surry reactor, these mechanisms are much weaker at Surry than at Peach Bottom. It is then not surprising that releases for the two accidents are different as follows:

Integral Releases After 10 hours of
Core Debris Concrete Interactions

Species	Surry	Peach Bottom
UO_2	6.5×10^{-3}%	1.3×10^{-2}%
La_2O_3	5×10^{-4}%	1.8%
CeO_2	0.1 %	2.9%
SrO	12 %	67%
BaO	9.7 %	48%

Table 2 Some Difference Between the Surry TMLB' and
The Peach Bottom AE Accidents

Parameter	Surry	Peach Bottom
Initial melt temp (K)	1807	2125
UO_2 mass (Kg)	79630	159391
Initial Zr mass (Kg)	6690	41070
Initial ZrO_2 mass (Kg)	13210	32990
Initial floor area (m^2)	57.55	32.17
Concrete type	basaltic	limestone
CO_2 in concrete (w/o)	1.5 ± 1.0	35.7 ± 1.0
H_2O in concrete (w/o)	5.0 ± 0.5	4.1 ± 0.5
Time after scram that melt/concrete attack begins (min)	157.3	126.26

As might be expected, the releases are greater for Peach Bottom because the melt was hotter for a longer time, the gas composition was strongly reducing for a longer period and gas generation was more intense.

Item 10: Describe the WITCH-GHOST test.

Response 10

The WITCH-GHOST tests at SNL are for VANESA validation and are separate-effects tests to address several issues that arise in formulating a model such as VANESA:

(1) Characterize aerosol particles formed per bubble burst and the size distribution of particles formed by bubble bursting at the surface of a melt.

(2) Determine if chemical effects drastically alter activity coefficients of melt species and consequently their volatility.

Mechanical aerosol formation is considered to be an important mechanism in the VANESA model. The modeling is based, however, on data for single bubbles passing through water. A legitimate question is whether or not such a model is applicable to bubbles passing through high temperature melts.

A first, exploratory test of mechanical aerosol generation has been done to develop test techniques (development of a bubbler for high temperature melts and a bubble counter). Qualitative indications are that particle sizes predicted by VANESA are quite good and particle numbers are not radically in error.

A second phase of the WITCH-GHOST procedure will examine the activity assumption for selected species. With the exception of a few species, melts are described in VANESA as ideal mixtures. At high temperatures this assumption may be adequate. But at temperatures less than about 2200°K one has to be concerned about non-idealities and the actual activity coefficients of melt constituents. Initially attention will focus on Na, I, Ba, and Sr in oxidic melts and Mo, Ag and Te in metallic melts.

The WITCH-GHOST tests are to be relatively small-scale, well-controlled tests. They cannot however be too small since wall effects on gas bubbles is a well-known phenomena that has plagued more than one study.

Currently it is anticipated that the WITCH-GHOST tests will use furnace-prepared and sustained melts of about 45 Kg mass. The melts will be sparged with gases at controlled rates with bubbles of known size, shape, and frequency. Bubble properties, melt surface tension and melt viscosity will be the primary variables in studies of mechanical aerosol formation. Melt composition, gas composition and temperature will be the primary variables in studies of melt constituent activities.

The WITCH-GHOST test will likely begin late in January 1985.

References

(1) D. A. Powers, Sustained Molten Steel/Concrete Interactions Tests, SAND77-1423, Sandia Laboratories, Albuquerque, NM, June, 1978.
D. A. Powers, "Sustained Molten Steel/Concrete Interactions Tests", Proc. of the Third Post-Accident Heat Removal Information Exchange, ANL-78-10.

(2) D. A. Powers and F. E. Arellano, Large-scale, Transient Tests of the Interaction of Molten Steel with Concrete NUREG/CR-2282, SAND81-1753, Sandia National Laboratories, Albuquerque, NM, Jan. 1982

(3) H. J. Sutherland et al., Acoustic Diagnostic Techniques for Post Accident Heat Removal Experiments, Proc. Int'l Conf. on Fast Reactor Safety and Related Physics CONF-761001 Volume IV, Aug. 1977

(4) H. J. Sutherland and L. A. Kent, Rev. of Scientific Instruments, 48 (1977)110

(5) H. J. Sutherland, Penetration of Molten Core Materials into Basaltic and Limestone Concrete. Proc. ENS/ANS Int'l Topical Mtg. on Nuclear Power Reactor Safety, Oct. 1978, Brussels, Belgium, Vol. 2

(6) D. A. Powers and F. E. Arellano, Direct Observation of Melt Behavior During High Temperature Melt/Concrete Interactions, NUREG/CR-2283, SAND 81-1754, Sandia National Laboratories, Albuquerque, NM, Jan. 1982

(7) R. Clift, J. R. Grace, and M. E. Weber, Bubbles, Drops and Particles, Academic Press, 1978

(8) I. Catton question posed to M. Reimann at the 6th Information Exchange Meeting on Debris Coolability, Los Angeles, CA., Nov., 1984

(9) M. Lee and M. S. Kazimi, "Interfacial Heat Transfer Between Bubble Agitated Immiscible Liquid Layers", Proc. 6th Information Exchange Meeting on Debris Coolability, Los Angeles, CA., Nov. 1984.

Primary References to the Thermochemical and Spectroscopic Properties of $LaO_{(g)}$.

LaO

[f] From band origins (25) as well as band heads (7) in $C-A^*$, the latter corrected for head-origin separations.
[g] From band heads in the 0-0 sequence of $C-X$ (6) after correcting for head-origin separations.
[k] Slightly different constants in (27).
[l] Large A-type doubling in $^2\Pi_{\frac{1}{2}}$: $\Delta\nu_{ef}(v=0) = +0.121(J+\frac{1}{2}) - \ldots$; in $^2\Pi_{3/2}$: $\Delta\nu_{ef}(v=0) = +0.80 \times 10^{-6}(J-\frac{1}{2})(J+\frac{1}{2})(J+3/2)$.
[j] $D_1 = 2.5 \times 10^{-7}$.
[k] Systems $G \rightarrow ?$ and $E \rightarrow ?$ of (7).
[l] $J'=0$ relative to $F''=0$ or $J''=0$.
[m] From band heads and calculated head-origin separations in $B-X$.
[n] Large spin doubling in $B\ ^2\Sigma^+$: $\Delta\nu_{12} = (-)0.256(N+\frac{1}{2})$; small hyperfine structure [see (28)].
[o] $A_0 = +862.6$.
[p] From band heads and calculated head-origin separations in $A-X$.
[q] Large A-type doubling in $^2\Pi_{\frac{1}{2}}$: $\Delta\nu_{ef} = +0.267(J+\frac{1}{2})$.
[r] $B_1(^2\Pi_{3/2}) = 0.3449$.
[s] From Q as well as P heads, the latter corrected for head-origin separations, in the 0-0 sequence of $C\ ^2\Pi_{\frac{1}{2}} - A^*\ ^2\Delta_{3/2}$.
[t] $D_1 = 2.5 \times 10^{-7}$.
[u] Matrix studies at 4 K (14)(19) confirm that $X\ ^2\Sigma^+$ is the ground state. See also (12)(13).
[v] Small spin doubling in $X\ ^2\Sigma^+$: $\Delta\nu_{12} = +0.0025_7(N+\frac{1}{2})$ (28); large hyperfine structure, $4b = 0.494$ (10)(26)(28).
[w] In Ar matrix at 4 K (14)(19).

(1) Jevons, PPS 41, 520 (1929).
(2) Meggers, Wheeler, JRNBS 6, 239 (1931); 9, 268 (1932).
(3) Piccardi, GCI 61, 127 (1933).
(4) Gatterer, RS 1, 153 (1942).
(5) Chupka, Inghram, Porter, JCP 24, 792 (1956).
(6) Gatterer, Junkes, Salpeter, Rosen, NBTOX (1957).
(7) Hautecler, Rosen, BCSARB 45, 790 (1959).
(8) Goldstein, Walsh, White, JPC 65, 1400 (1961).
(9) Tawde, Chandratreya, CS 30, 137 (1961).
(10) Åkerlind, AF 22, 65 (1962).
(11) Ortenberg, Glasko, Dimitriev, SAAJ 8, 258 (1964).
(12) Berg, Wharton, Klemperer, Büchler, Stauffer, JCP 43, 2416 (1965).
(13) Brewer, Walsh, JCP 42, 4055 (1965).
(14) Kasai, Weltner, JCP 43, 2553 (1965).
(15) Smoes, Drowart, Verhaegen, JCP 43, 732 (1965).
(16) Ames, Walsh, White, JPC 71, 2707 (1967).
(17) Coppens, Smoes, Drowart, TFS 63, 2140 (1967).
(18) Drowart, Pattoret, Smoes, PBCS, No. 8, 67 (1967).
(19) Weltner, McLeod, Kasai, JCP 46, 3172 (1967).
(20) Carette, Houdart, CR B 271, 110 (1970).
(21) Murthy, Murthy, JP B 3, L15 (1970); 5, 714 (1972).
(22) Suárez, JP B 3, 729 (1970); CPL 16, 515 (1972).
(23) Uy, Drowart, HTS 2, 293 (1970).
(24) Carette, Houdart, CR B 272, 595 (1971).
(25) Green, JMS 38, 155 (1971).
(26) Green, CJP 49, 2552 (1971).
(27) Green, JMS 40, 501 (1971).
(28) Bacis, Collomb, Bessis, PR A 8, 2255 (1973).
(29) Ackermann, Rauh, JCP 60, 2266 (1974).
(30) Marañon, Suárez, SpL 7, 303 (1974).
(31) Rauh, Ackermann, JCP 60, 1396 (1974).
(32) Schoonveld, Sundaram, ApJ(Suppl.) 27(246), 307 (1974).

Selection of Plants and Accident Sequences

The objective of the BMI-2104 study at Battelle Columbus was to develop the methodology for improved, best-estimate source term calculations, and to demonstrate that methodology for a spectrum of severe accident conditions. The methodology is to employ improved models for the release of fission products from fuel, transport and deposition in the primary system, attenuation by engineered safety systems, and transport and retention in the containment and/or other structures. It was apparent at the time of the invitation of this task, that the methodology was sufficiently detailed to require selection of specific plants and accident sequences for the sample calculations to be performed. The plants selected for these calculations, therefore, were chosen on the basis of: (1) ready availability of the design details required for the analysis, (2) specific plant design features (e.g., suppression pools, ice condenser), and (3) availability of other studies to facilitate comparisons. With these criteria, the following plants were selected: (1) Surry, a PWR with a subatmospheric containment, being the PWR plant analyzed in the RSS, (2) Peach Bottom, a BWR with a MARK I type pressure suppression containment also analyzed in the RSS, (3) Sequoyah, a PWR with an ice condenser type containment, (4) Grand Gulf, a BWR with a distinct new (MARK III) containment design, and (5) Zion, a PWR with a very large high strength containment typical of many newer PWRs analyzed by the IDCOR Study. (The original scope of the BMI-2104 study did not include a MARK II pressure suppression containment, as it was thought that the physio-chemical environment for this design would be comparable to the MARK I containment.)

Similar to the selection of specific plants, discussed above, the accident sequences to be analyzed with the new methodology were selected to provide a wide spectrum of physio-chemical conditions, in order to demonstrate the applicability of the newly developed models for the full spectrum of accidents.

For this reason, accident sequences were selected from general groups such as: large LOCAs, small LOCAs, transients, sequences expected to minimize and maximize the effects of engineered safety features, accidents likely to result in early or late containment failure, and, for each plant, a sequence which (on the basis of RSS insights) is likely to be a significant contributor to the accident risk.

For the SURRY plant, for example, the AB sequence (a large LOCA with loss of all AC power) was selected as a sequence resulting in the most rapid depressurization, core heat-up, and containment pressurization. In addition, specific parameters in the analysis were selected to maximize the challenge to the containment by rapid hydrogen burning. If the new methodology for the analysis of fission product behavior can be demonstrated for this sequence, therefore, there is a reasonable expectation that the methodology is viable for predictions of similar fast, early containment failure sequences. It should be noted that the significance of this accident sequence lies entirely in its challenge to the methodology, as it is generally agreed that its risk significance is negligible, owing to its vanishingly small probability.

In contrast, the small LOCA sequence selected for analysis (S_2D) is well over a thousand times more likely to occur. As a result of the operation of containment sprays, however, this sequence is not likely to result either in containment failure, or large source terms. The operation of the containment spray system, however, present a unique challenge to the ability of the new models to predict the behavior of aerosols in the containment.

An entirely different pathway for potential fission product transport to the environment exists for the V sequence, in which a rupture in a pipe carrying primary coolant outside the containment is postulated. This scenario, therefore, involves the bypass of the containment, with the fission products released to the auxiliary building, and was included for this reason. As this sequence was thought to be independent of containment design, it was analyzed for one plant (i.e., SURRY) only.

The TMLB sequence (i.e., a transient with loss of AC power, similar to a "station blackout" scenario) was included in the SURRY set of sequences because it was believed to be the major contributor to accident risk at SURRY.

Similar reasoning led to the selection of the sequences for the other plants, with the additional intention of limiting the total number of analyses to manageable proportions. The resulting list of plants and accidents is shown in the attached table.

Table 4.1

Accident Sequences and Plants Analyzed Using Current Methodology

	Plant	Description: Type	Description: Containment Design	BMI-2104 Volume	Accident Sequences Analyzed
1.	SURRY	PWR	Large, Dry Subatmospheric	I and V (Recalculations)	AB TMLB' S_2D V
2.	PEACH BOTTOM	BWR	MARK I	II	AE TC TW
3.	GRAND GULF	BWR	MARK III	III	TC TPI TQUV S_2E
4.	SEQUOYAH	PWR	Ice Condenser	IV	S_2HF TML TMLB'
5.	ZION	PWR	Large, Dry	VI	TMLB' S_2D

E.H.

Battelle
Columbus Laboratories
505 King Avenue
Columbus, Ohio 43201
Telephone (614) 424-6424
Telex 24-1454

June 21, 1984

Summary (9.c.1)

Dr. Eric Haskin
Division 9411
Sandia National Laboratories
Albuquerque, New Mexico 87185

Dear Eric:

Enclosed for your review is a draft of the "PWR Standard Problem - Ice Condenser Design".

Since this report is intended to reflect our consensus views, your review and comment would be appreciated. Specifically, any major misinterpretations or omissions regarding your analyses should be called to my attention. As you will note, I have tried to work with the tables and figures that were available to me; I would appreciate clearer copies of the figures and tables that you would like to see included in the report.

I am planning to include in the appendix selected plots and tables for each of the specific calculations that we conducted; these are not included with the current draft, but are identical to what you have seen before. If you would like me to do the same for your calculations, please forward them to me; otherwise, you may send your individual report directly to the NRC.

I apologize for the delay in getting this draft to you, and would greatly appreciate your early response.

Sincerely,

Peter Cybulskis

PC/lij

Enclosure

cc: M. Silberberg, NRC
J. Rosenthal, NRC
J. Telford, NRC
M. Cunningham, NRC

DRAFT

PWR STANDARD PROBLEM - ICE CONDENSER DESIGN

INTRODUCTION

The objective of the Containment Loads Working Group (CLWG) is to develop an updated technical position on the relatively short term (few hours duration) containment pressure and temperature loading following reactor vessel failure. A way of developing an understanding of the problem is to have a number of experts analyze well defined situations representative of the conditions expected during the course of severe reactor accidents. Comparison of the results of such analyses would bring into focus differences in the understanding of the phenomena and methods used to treat them as well as areas of agreement among the analysts. The analysis of a series of "standard problems" was the approach selected by the CLWG.

This report describes the PWR Standard Problem for the Ice Condenser containment design and describes the results obtained for this problem by Battelle.s Columbus Laboratories and Sandia National Laboratories. This report is intended to present the concensus views of the two groups working on this problem.

APPROACH

The TMLB accident sequence was selected as the basis for analysis in the ice condenser containment design. Based on earlier analyses, e.g., BMI-2104 and others, which had indicated a potential vulnerability of this design to hydrogen burns, the CLWG standard problem analyses focused on the loadings due to this source. In the TMLB sequence the hydrogen igniters typically provided in containments of this type would not be

operable due to the assumed loss of electric power, thus a variety of hydrogen ignition assumptions could logically be investigated for this sequence.

MARCH 2 analyses were used to determine the in-vessel hydrogen generation and release to the containment for the purposes of the subsequent assessment of the effect on the containment of resulting hydrogen burns. The input for the MARCH 2 analyses used the Sequoyah plant design as the model and the actual input parameters utilized were similar to those of the BMI-2104 calculations for this type of design. One point of difference from the earlier calculations was the use of revised values for the volume of water on the containment floor before spillover into the reactor cavity and the volume of the reactor cavity; the revised values were provided by TVA, the owner of the Sequoyah plant.

Using the MARCH 2 calculated rates of hydrogen generation and release to the containment, Sandia National Laboratories and Battelle's Columbus Laboratories conducted independent calculations of the occurrence and effects of subsequent hydrogen burns in the containment. The specific approaches used by each of the two laboratories will be described later. The analyses performed by the two laboratories included consideration of: various hydrogen ignition criteria, effects of varying the in-vessel hydrogen production, effects of the timing and rate of hydrogen release from the primary system, and variations in the magnitude of the steam spike due to the debris-water interaction following vessel bottom head failure. The variations in each of these parameters that were considered are discussed below.

As was noted previously, in the TMLB sequence chosen as the basis of analysis the hydrogen igniters would not be available, and ignition, if it takes place, could conceivably take place at any time during the accident sequence. In the initial set of calculations undertaken as part of this standard problem, ignition was assumed whenever the hydrogen concentration in any compartment of the containment reached preselected levels; specifically, hydrogen concentrations of 8, 12, and 30 v/o were assumed for ignition. The occurrence of ignition was still subject to other constraints, such as the availability of oxygen and absence of inerting due to diluents. Later calculations sought a somewhat more mechanistic basis for the occurrence of ignition, and were tied to the timing of the failure of the vessel head, with the release of the hot corium being the source of ignition either immediately upon release from the primary system or at some time later. Additional calculations were performed in which ignition was assumed at low hydrogen levels, e.g., 4.1 v/o, as well as without any hydrogen burning.

In the base case MARCH 2 calculation approximately 40 per cent of the Zircaloy cladding was predicted to have reacted with steam during the in-vessel phase of the accident to produce hydrogen. For purposes of investigating sensitivities of the containment response, additional cases were considered in which the reaction of the Zircaloy was arbitrarily forced to completion in the primary system, as well as some cases in which the in-vessel modeling assumptions were changed to produce less than the base case extent of Zircaloy reaction.

In a normal MARCH calculation the failure of the reactor vessel bottom head is assumed to be a large opening. For transient accident sequenses such as the one considered here, a normal MARCH calculation typically predicts that very little of the hydrogen generated in-vessel is released to the containment prior to bottom head failure; thus the latter is typically followed by the release to the containment of a large quantity of hydrogen. Such rapid releases of hydrogen to the containment could have an undue influence on the prediction of the effects of hydrogen burning. As part of the standard problem analyses some alternated assumptions regarding the timing and rate of hydrogen release to the containment were also considered. Specifically, the situation where the collapse of the molten core into the vessel bottom head leads to the early failure of the head via a small hole, such as may be associated by the melting of a pnetration, was considered. In the MARCH analyses this situation was actually modeled by the opening of the relief valve at the time of the start of core collapse; this permitted the release of the hydrogen from the primary system to start prior to the general failure of the head and the release of the core debris to the reactor cavity.

In a typical analysis of the TMLB sequence the failure of the vessel bottom head is followed by the discharge of the accumulator water and the subsequent interaction of the core debris with this water. The large steam spikes that are typically associated with the latter interactions can result in the rapid transport of hydrogen from the lower compartment to the upper compartment of the ice condenser containment. The subsequent burning of the

hydrogen in the upper compartment can pose serious challenges to containment integrity. In addition to such a large steam spike which was considered in the base case MARCH analysis, alternate cases were considered in which only minimal interaction between the core debris and water in the reactor cavity were assumed. In these cases the debris were assumed not to fragment, but remain as a coherent mass; this assumption leads to the early attack of the concrete by the core debris, with heat transfer to the overlaying water layer by film boiling and radiation.

In the analyses conducted for t e purposes of this standard problem no assumptions were made regarding the pressure or temperature levels at which the containment would fail. The analyses were performed as if the containment had infinite strength in order to develop a pisture of the magnitude of the loads that would be predicted under the variety of modelling assumptions discussed above.

Approach Taken by Battelle

All of Battelle's calculations for the Ice Condenser PWR Standard Problem were performed with the MARCH 2 code. Thus the MARCH calculations were used not only to define the in-vessel hydrogen generation and release to the containment, but also to evaluate the subsequent behavior of the hydrogen in the containment. The BURN subroutine in MARCH is used to determine flammability, flame speeds, flame propagation between compartments, etc.; this subroutine was basically developed by Sandia and has been adapted for incorporation into the MARCH code. The ignition and burning

criteria incorporated into the BURN subroutine are very similar to those in Sandia's HECTR code. The MACE subroutine in MARCH describes the containment response, including the effects of hydrogen burning as defined by the subroutine BURN. The MACE routine determines mass and energy transfers between compartments on the assumption that the pressures in the various containment compartment are equal. This approximation is believed to be a valid one except for extremely rapid transients, e.g., detonation. The pressure equilibriation assumption is somewnat unique to the MARCH code and is not widely used.

In the MARCH analyses the ice condenser containment was modeled as a four compartment system. The four compartments modeled were: the dead end spaces in the lower compartment, the main area of the lower compartment, the upper plenum of the ice condenser, and the operating floor and dome volume. The containment compartmentalization is illustrated in Figure 1. In MARCH the ice condenser itself is modeled in the junction between two compartments, in the present case between the main volume of the lower compartment and the upper plenum of the ice condenser. The performance of the ice condenser is described by specifying the exit temperature from the ice condenser: the values used in MARCH are based on the experimental results with a segment of a full scale system. Only one way flow through the ice condenser is permitted in MARCH.

Approach Taken by Sandia

Sandia's analyses utilized the in-vessel hydrogen generation and release to the containment as predicted by MARCH as input to the HECTR code: the latter described hydrogen burning and the

resulting response of the containment. The HECTR code was specifically developed for addressing issues related to hydrogen burning during severe reactor accidents and represents a much more detailed treatment of the problem than afforded by the MARCH code. Some of the key features of HECTR of interest to the evaluation of the Ice Condenser PWR Standard Problem are noted below.

Mass and energy transfers in HECTR are based on pressure driven as well as buoyant flows, accounting for flow resistances and one way ice condenser doors, including time required for these doors to close. HECTR is capable of modeling series as well as parallel flow paths among compartments: for the ice condenser containment this included consideration of the flow from the lower to the upper compartment that bypassed the ice bed. The ice condenser compartment is explicitly modeled in the HECTR calculations, including a steam condensation model that is a function of the flow through the ice bed.

In the HECTR analyses the ice condenser containment was modeled by nine interconnected volumes. these included: the dead spaces in the lower compartmenr, the main area of the lower compartment, the lower plenum of the ice condenser, four volumes in the ice bed, the upper plenum of the ice condenser, and the operating floor and dome volume. This compartmentalization is illustrated in Figure 2. Bypass of the ice condenser through the floor drain return lines was considered, as was the finite time required to close the ice condenser one way doors.

It was noted previously that the hydrogen ignition and flame

propagation criteria in HECTR and the BURN subroutine in MARCH have a common origin and are very similar. Once hydrogen burning is initiated, the HECTR modeling includes radiation heat transfer from the flame to structures in the compartment; MARCH does not include a flame radiation model.

RESULTS

MARCH 2 Analyses of In-Vessel Accident Progression

MARCH 2 analyses were used to predict the in-vessel hydrogen generation and its release to the containment. The MARCH calculations for this standard problem were very similar to those conducted for BMI-2104, with the exception of some updated input on the volume of water on the containment floor before overflow into the reactor cavity. The in-vessel modeling (MARCH subroutine BOIL) options and assumptions in the base case calculation were identical to those of BMI-2104. At the time of vessel bottom head failure approximately 49 per cent of the Zircaloy cladding was predicted to have reacted with steam to generate hydrogen. Most of the hydrogen generated in-vessel was retained in the reactor coolant system up to the time of vessel failure and was released rapidly upon failure together with the contained quantity of high pressure steam.

Table I gives the accident event times for a representative MARCH analysis for the TMLB sequence as obtained by Sandia. Figure 3 gives the corresponding steam source to the containment, and Figure 4 presents the hydrogen input into the containment. As illustrated in Figure 3, the steam input into the containment consists of two components: the first is the release of the high pressure steam stored within the primary coolant system, and the second is the result of the interaction of the core debris with the accumulator water in the reactor cavity. The hydrogen source also is made up of two components: the hydrogen produced in-

vessel during the core melting phase, and the hydrogen generated during the debris-water interaction. Figure 4 illustrates that the former is substantially larger than the latter under the conditions of this analysis.

Figures 5 and 6 give the containment pressures and temperatures for the foregoing case as calculated by HECTR without any hydrogen burning. Figure 7 illustrates the ice remaining in the ice condenser as a function of time.

Analysis of Containment Response Without Hydrogen Burning

Before presenting specific results of the hydrogen burning analyses, it may be instructive to consider the predictions of containment conditions without burning; this may be useful background in the understanding of analyses with hydrogen burning. Figure 8 illustrates the containment pressure response in the absence of any burning as calculated by MARCH. Note that this particular calculation was carried out for a long time into the accident sequence; our principal interest is in the time period of a few hours following reactor vessel failure, or perhaps to about 300 minutes on this figure. Vessel head failure is predicted at about 150 minutes, with a containment pressure of about 30 psia immediately after head failure. The predicted containment pressure is relatively low even though the failure of the vessel head is followed by rapid debris quench due to the effectiveness of the ice condenser. Comparison of Figures 5 and 8 shows the difference between the MARCH and HECTR predictions of the containment responses in the absence of burning. The reasons for these differences will be discussed later. Figures 9-12

present the composition histories of the four compartments in terms of the mole fractions of steam, hydrogen, and oxygen. Nitrogen is the other constituent of the containment atmosphere that is not explicitly shown in these figures; after the onset of the corium-concrete interaction there may also be some carbon monoxide and carbon dioxide present. In these figures, Volume 1 represents the dead end spaces in the lower compartment, Volume 2 is the main area of the lower compartment, Volume 3 represents the upper plenum of the ice condenser, and Volume 4 is the dome region and operating floor. Figure 9 indicates that the dead end compartments would be expected to be nonflammable due to low hydrogen concentration, but possibly also due to high steam concentration later in time. Figure 10 illustrates that the main volume of the lower compartment would be inerted essentially throughout the time period of interest by the very high steam concentrations predicted. Figure 11 shows very high hydrogen concentrations in the upper plenum of the ice condenser immediately following vessel failure. The high hydrogen flows are seen to temporarily reduce the oxygen level in this compartment, but there is significant overlap between high hydrogen and near normal oxygen concentrations. The oxygen level is seen to build up again after the debris quenching process has run its course. The steam concentration in the upper plenum of the ice condenser is maintained at very low levels by the implied effectiveness of the ice condenser. Figure 12 indicates that flammable conditions would be established in the upper compartment shortly after head failure and maintained for the

time duration of interest. It should be emphasized that the results presented in the foregoing figures are based on no burning, and that the assumption of burning at any stage in the calculation would alter the subsequent observations. These figures do illustrate the types ofcomposition changes that are predicted in the analyses with burning considered, and lend insight on the reasons why certain compartments are flammable at some times and not at others.

Results od Hydrogen Burning Analyses

Tables II and III summarize the specific cases evaluated by Sandia and Battelle, respectively; further details on the individual cases are provided in the appendices. Table IV compares the results of the two sets of calculations for a number of key cases. Some general observations on the results of the Ice Condenser PWR Standard Problem will be given here. A discussion of the differences between the MARCH and HECTR predictions will be given in a later section.

The calculations performed for the TMLB sequence in an ice condenser containment design indicate that the lower portions of the containment will be inerted with respect to hydrogen burning for major portions of the accident sequence. The upper portions of the ice condenser, particularly the upper plenum, and the dome region of the containment would be expected to contain flammable compositions shortly after head failure as well as thereafter. Since, by definition, electric power is not available in this sequence, hydrogen igniters would not be available to control the buildup of high concentrations of hydrogen. Thus ignition could

effectively be a random event. The discharge of the hot core debris from the reactor vessel at the time of vessel head failure is often cited as a likely source of ignition. In the analyses considered here, however, the lower compartment was typically found to be inerted by high steam concentrations at the time of head failure. Thus the hot core debris would not necessarily be an effective ignition source unless some of the debris found their way into the upper compartment without first being cooled.

For the above reasons, a variety of ignition criteria were examined during these analyses: these included ignition on hydrogen concentration, on vessel breach, and at various time delays after vessel breach. Given ignition, a number of burns were typically predicted. Burning was typically predicted to start in the upper portions of the ice condenser compartment and, as long as the burning was confined to the ice condenser, very low containment pressure loads were found. In essentially all the cases considered, however, the burning was eventually predicted to propagate from the ice compartment to the upper dome region. When the latter occurred, substantial pressure rises were calculated.

Some of the sensitivities of the predicted containment loads on the variables considered in the analyses are discussed below. The predicted peak containment pressure loads were found to increase with the extent of in-vessel hydrogen production. This is an expected observation since the greater in-vessel production would lead to correspondingly higher hydrogen concentrations in

the various compartments of the containment.

DRAFT

The predicted peak containment pressures were found to be sensitive to the timing of ignition, with delays in the timing of ignition leading to higher peak pressures. This again is an expected result, since the longer the time to ignition, the more time for hydrogen to build up in the upper portions of the containment. Thw peak containment pressures were also found to increase with the magnitude of the steam spike following reactor vessel breach. The larger the steam spike the more of the hydrogen can be swept into the upper compartment: the large containment loads are always associated with burns that propagate into the upper compartment.

The dead end spaces of the lower compartment were generally predicted to be nonflammable, or have hydrogen concentrations barely into the flammable range. Thus minimal burning would be predicted in this part of the containment under the conditions of the present analyses. Since most of the containment penetrations are believed to be located in these areas, it may be inferred that overtemperature challenges to containment penetrations do not constitute a major threat to containment integrity.

The hydrogen concentrations in local regions were predicted to reach detonable proportions in a number of the cases considered. Neither HECTR nor MARCH can treat hydrogen detonations and are limited to the assumption of deflagration type behavior. Thus the possible implications of hydrogen detonations, should they occur, have not been addressed in the present studies.

DIFFERENCES BETWEEN MARCH AND HECTR MODELING

DIFFERENCES BETWEEN MARCH AND HECTR MODELING OF ICE CONDENSER CONTAINMENTS

It has been noted that there are a number of differences between the MARCH and HECTR treatments of ice condenser containments. Some of the principal differences and the implications of these differences on the predicted results will be discussed in this section.

The MACE routine in MARCH which treats containment behavior is basically limited to series flow paths: this means that all the flow from the lower compartment to the upper compartment passes through the ice condenser. HECTR models series as well as parallel flow paths; for ice condenser containments this includes consideration of some flow from the lower compartment to the upper compartment through the floor drains, thus bypassing the ice bed.

MARCH treats the ice condenser as a heat exchanger in the junction between two compartments. The performance of the ice condenser is described by specifying the exit stream temperature from the ice bed; the values incorporated into MARCH are based on the large scale experiments conducted in the course of the development of this containment concept. In the analyses conducted here this model results in the condensation of essentially all the steam passing through it. HECTR explicitly models the ice condenser by a series of compartments, including a steam condensation model that takes into account the rate of heat transfer between the fluid stream and the ice. The HECTR model permits more steam to pass through the ice bed without condensing than does the MARCH model.

The transfer of mass and energy between compartments in MARCH is,

with some exceptions, based on the assumption of pressure equilibration among compartments. This is believed to be a reasonable approximation except for very rapid transients, e.g., detonation. This approximation has been adopted in order to improve the efficiency of the computations and is somewnat unique to MARCH. HECTR models transfers between compartments due to pressure as well as buoyancy differences, accounting for flow resistances, one way ice condenser doors, the finite time required for these doors to close, etc.

The above key differences between the MARCH and HECTR treatments of the ice condenser containment are believed to be the reasons for the differences in the predicted results. In comparing the pressures predicted by the two codes in the absence of any burning, Figures 5 and 8, it can be seen that the HECTR modeling leads to higher containment pressures than does the MARCH treatment. This difference is consistent with the above discussion of differences. The higher pressures predicted by HECTR prior to burning are also manifested when burning takes place. The HECTR burn pressures start from a higher level than do those in MARCH. Also, the higher preexisting presures imply that a larger amount of hydrogen must be accumulated in any compartment to reach a given volumetric concentration of hydrogen.

CONCLUSIONS

Based on the analyses of the Ice Condenser PWR Standard Problem discussed above, the following observations can be made:

For the accident sequence considered, ignition of the hydrogen-air mixtures is effectively a random event; ignition is not assured even after vessel breach due to steam inerting of the lower compartment and lower portions of the ice condenser.

Assuming the availability of an ignition source, burning was typically found to start in the ice condenser, but generally was predicted to eventually propagate to the upper compartment.

When burning was confined to the ice condenser compartment, the resulting overall pressures were small; propagation of the burning to the upper compartment led to the prediction of large pressure rises.

The calculated peak pressure loadings were found to be sensitive to the timing of ignition, with longer delays to ignition leading to higher predicted peak pressures.

The predicted peak pressures in the containment were found to increase with increasing extent of in-vessel Zircaloy oxidation.

The predicted peak containment pressures were found to increase with increasing magnitude of the ex-vessel steam spike following vessel breach.

Locally detonable compositions were found to be possible under the conditions and assumptions of these analyses: the

effects of possible detonations were not considered in the present analyses.

A number of differences between the approaches used by the two groups analyzing this problem were noted. These differences lead to differences in the specific values in the loadings predicted, but the overall trends in predicted behavior were found to be very similar,

DRAF

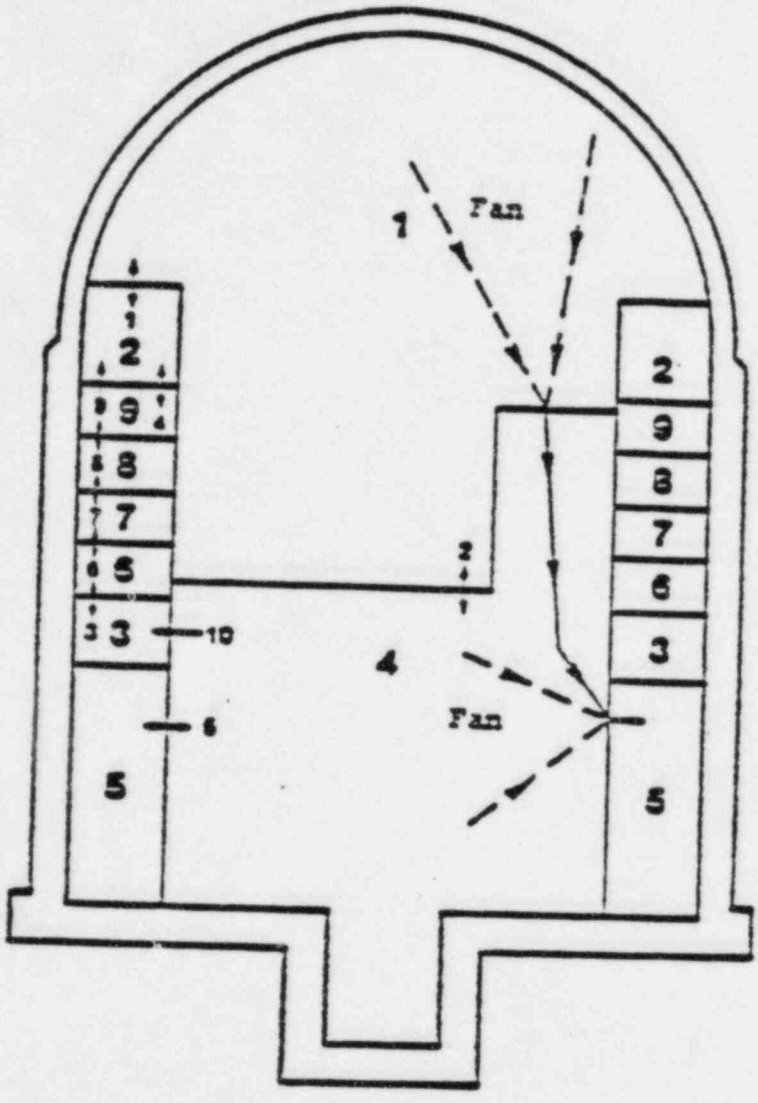

KEY

1 - Compartment Number

1 - Flow Junction Number

—— - One-way Flow Junction

⟷ - Two-way Flow Junction

Figure 2. HEGTR ice-condenser containment model.

DRAFT

Table I

MARCH 2.0 CHRONOLOGY FOR CLWG
ICE CONDENSER CONTAINMENT STANDARD PROBLEM

EVENT	TIME(S)
1. STM GEN DRY	3885
2. CORE UNCOVER	5550
3. START MELT	7350
4. CORE SLUMP	8640
5. START HEAD HEATUP	8745
6. BOTTOM HEAD FAIL	9465

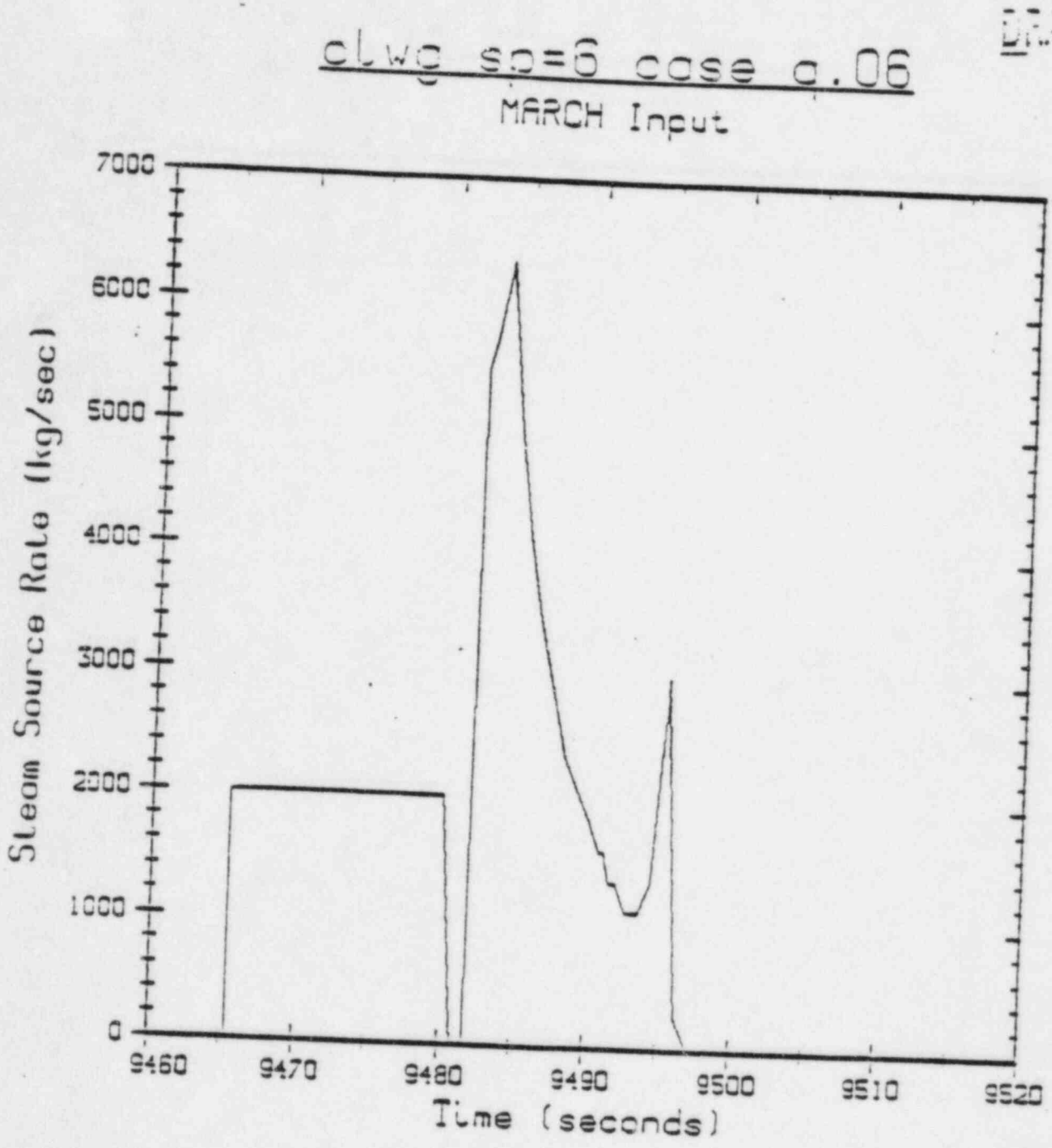

Figure 3

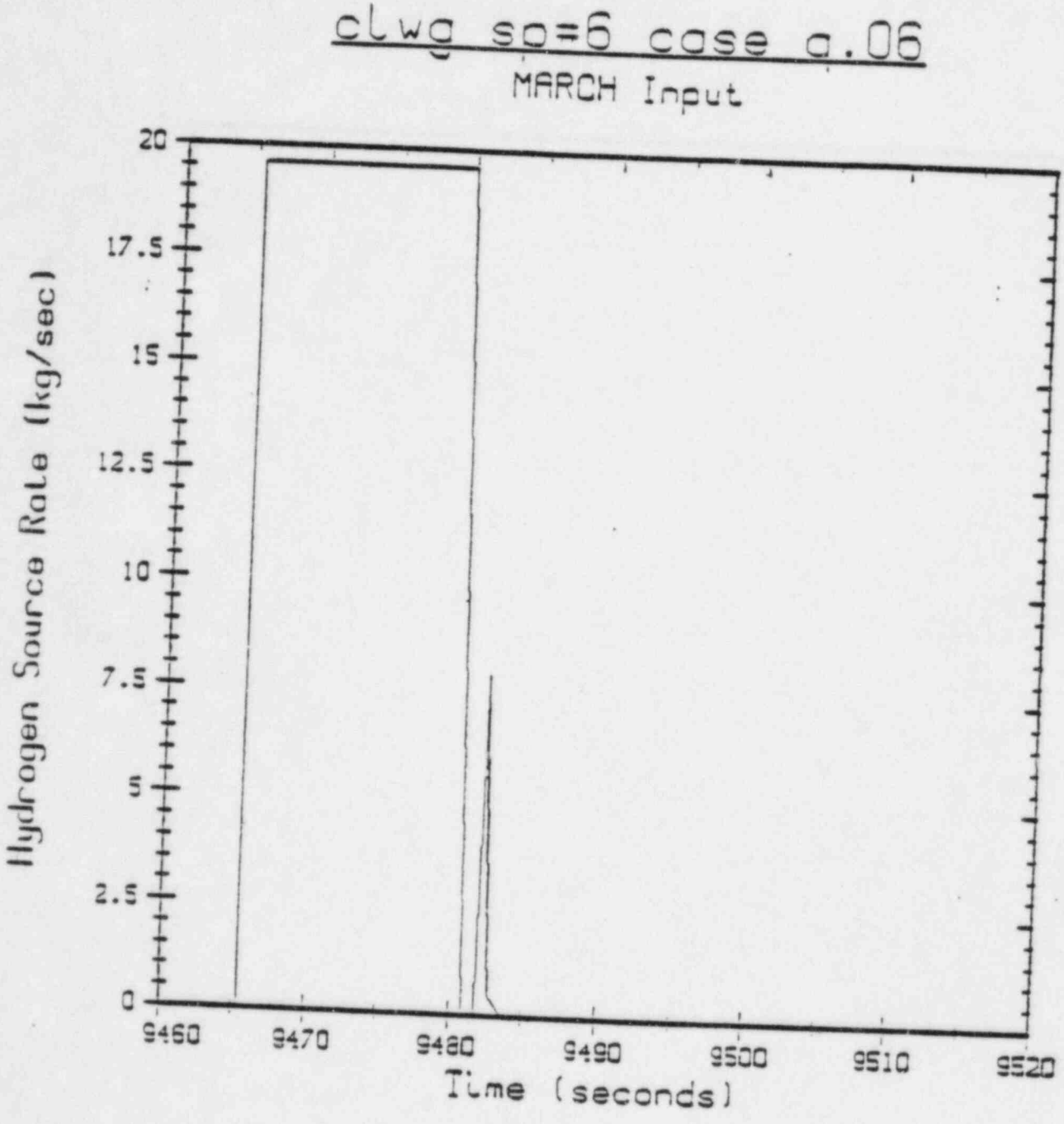
clwg sp=6 case a.06
MARCH Input
Hydrogen Source Rate (kg/sec)
20
17.5
15
12.5
10
7.5
5
2.5
0
9460
9470
9480
9490
9500
9510
9520
Time (seconds)

Figure 4

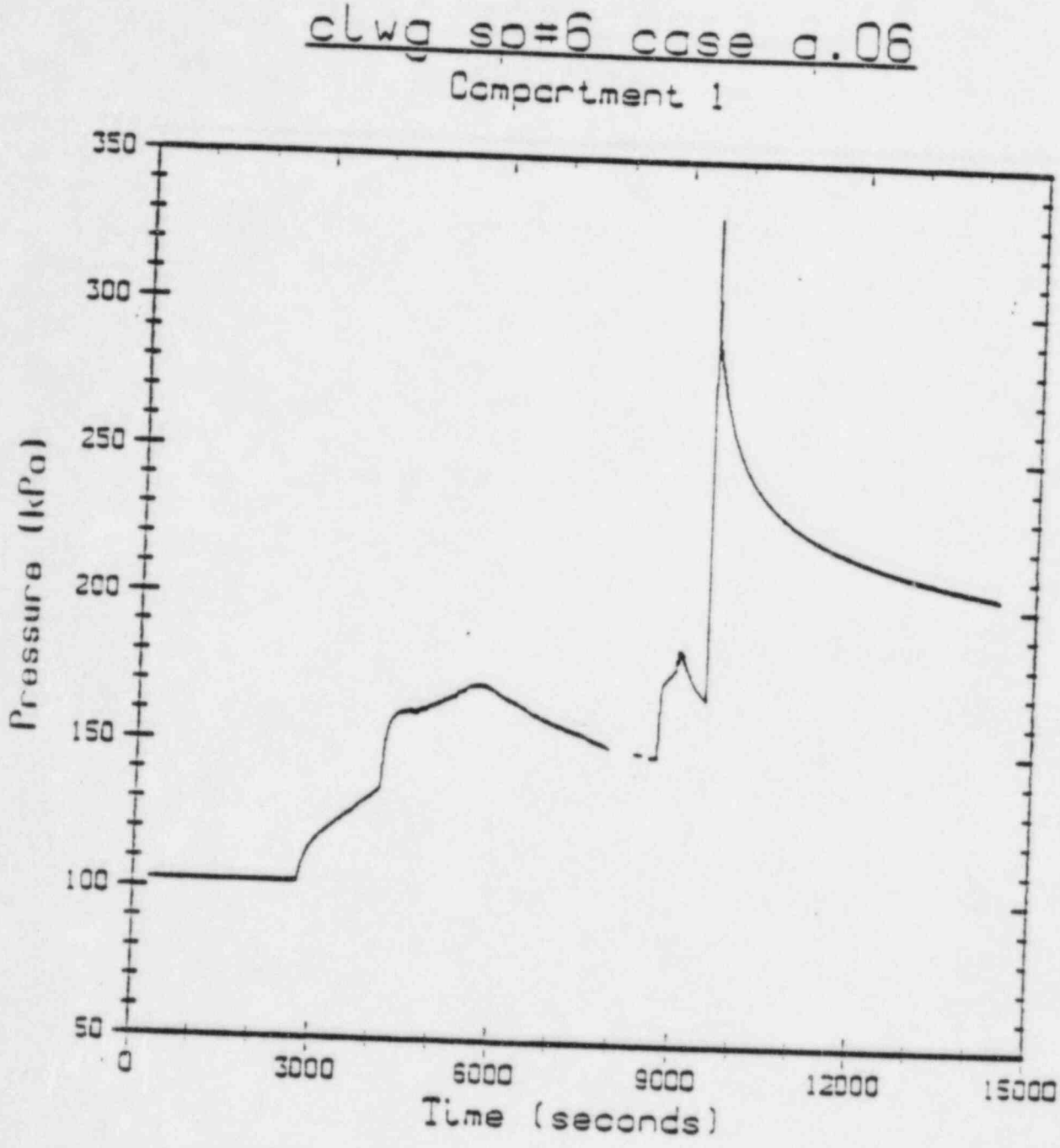
clwg sp=6 case a.06
Compartment 1
Pressure (kPa)
350
300
250
200
150
100
50
0
3000
6000
9000
12000
15000
Time (seconds)

clwg sp=6 case a.06

Compartment 4

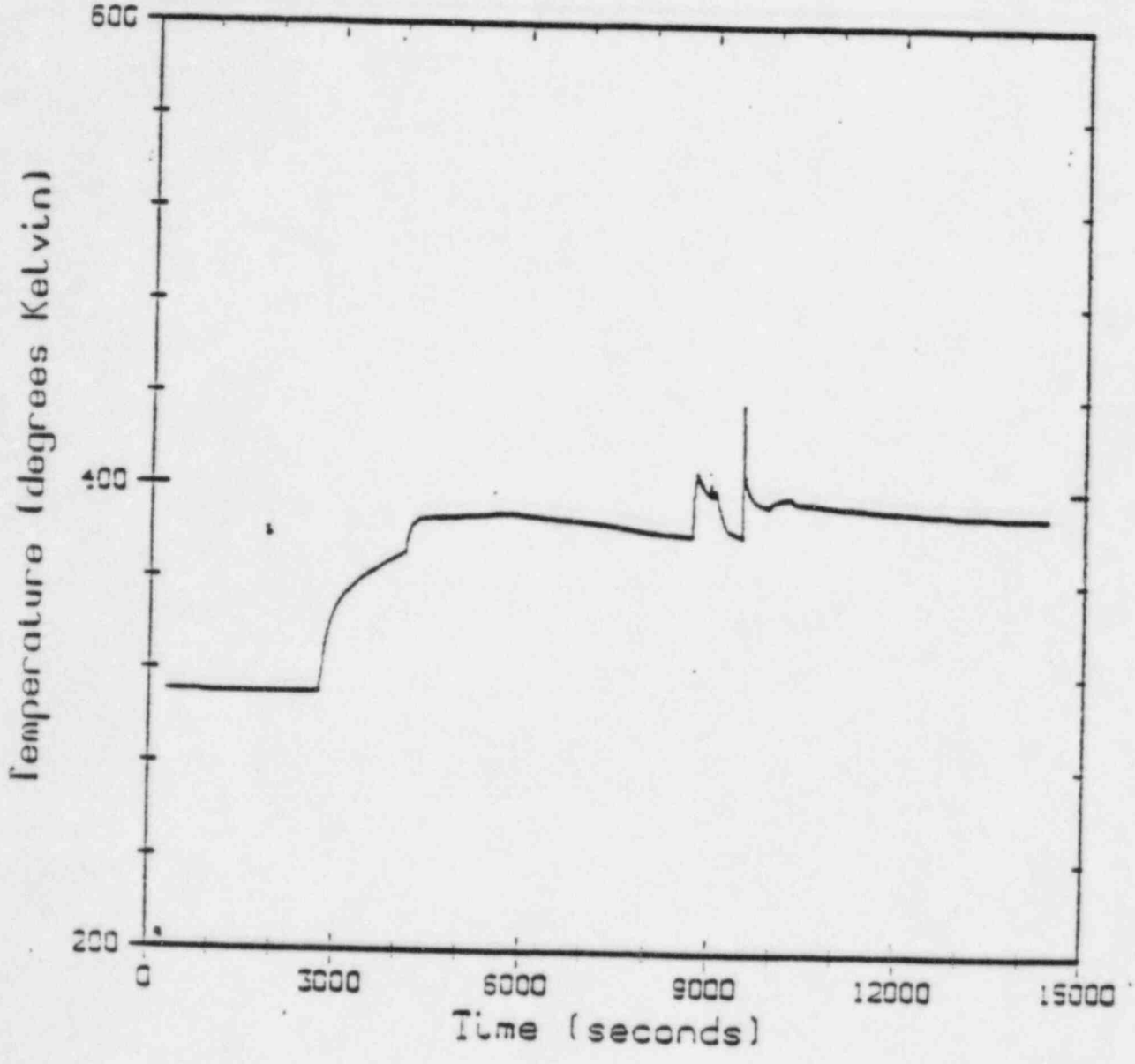

Figure 6

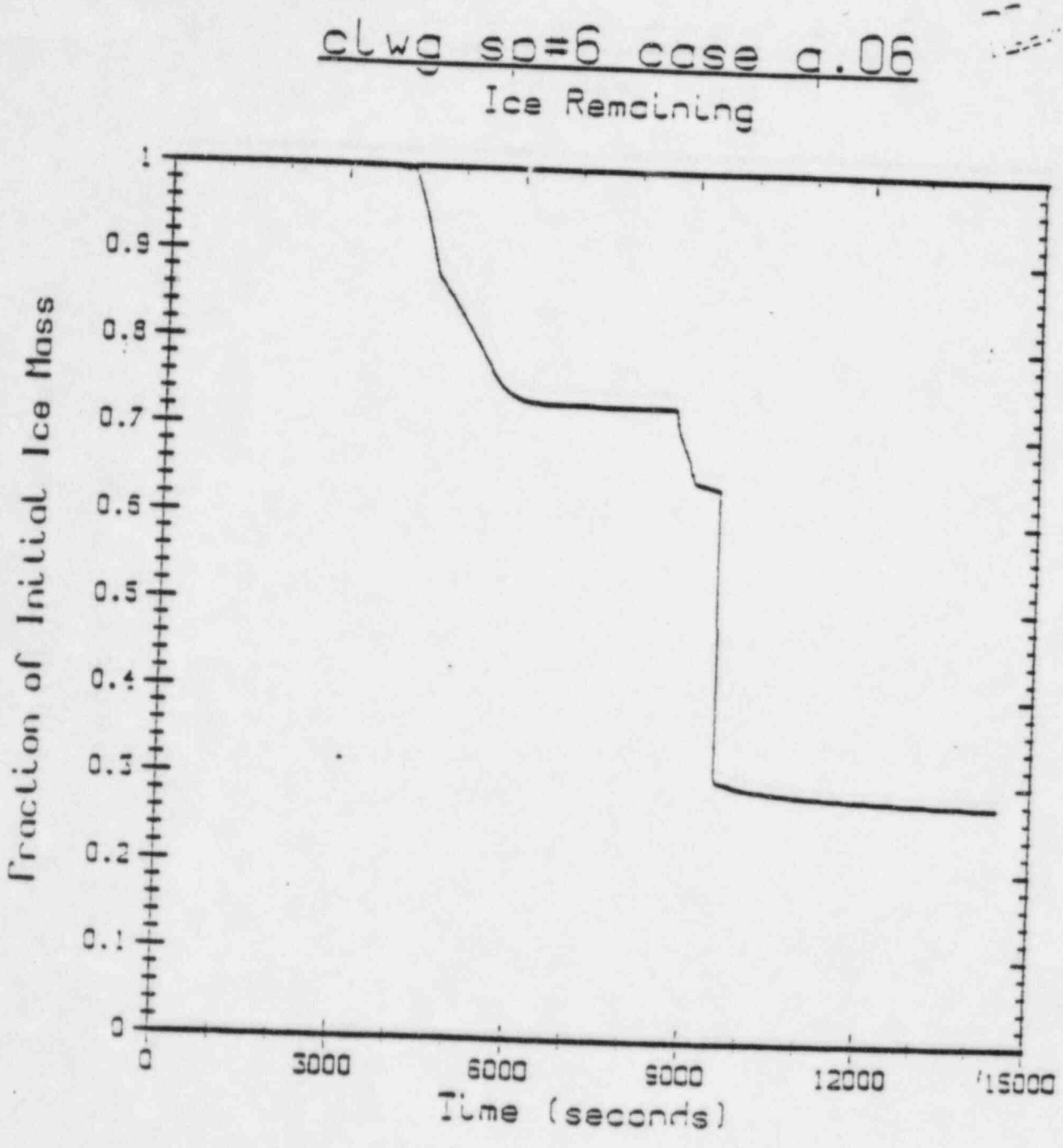
clwg sp=6 case a.06
Ice Remaining
Fraction of Initial Ice Mass
1
0.9
0.8
0.7
0.6
0.5
0.4
0.3
0.2
0.1
0
0
3000
6000
9000
12000
15000
Time (seconds)

Figure 7

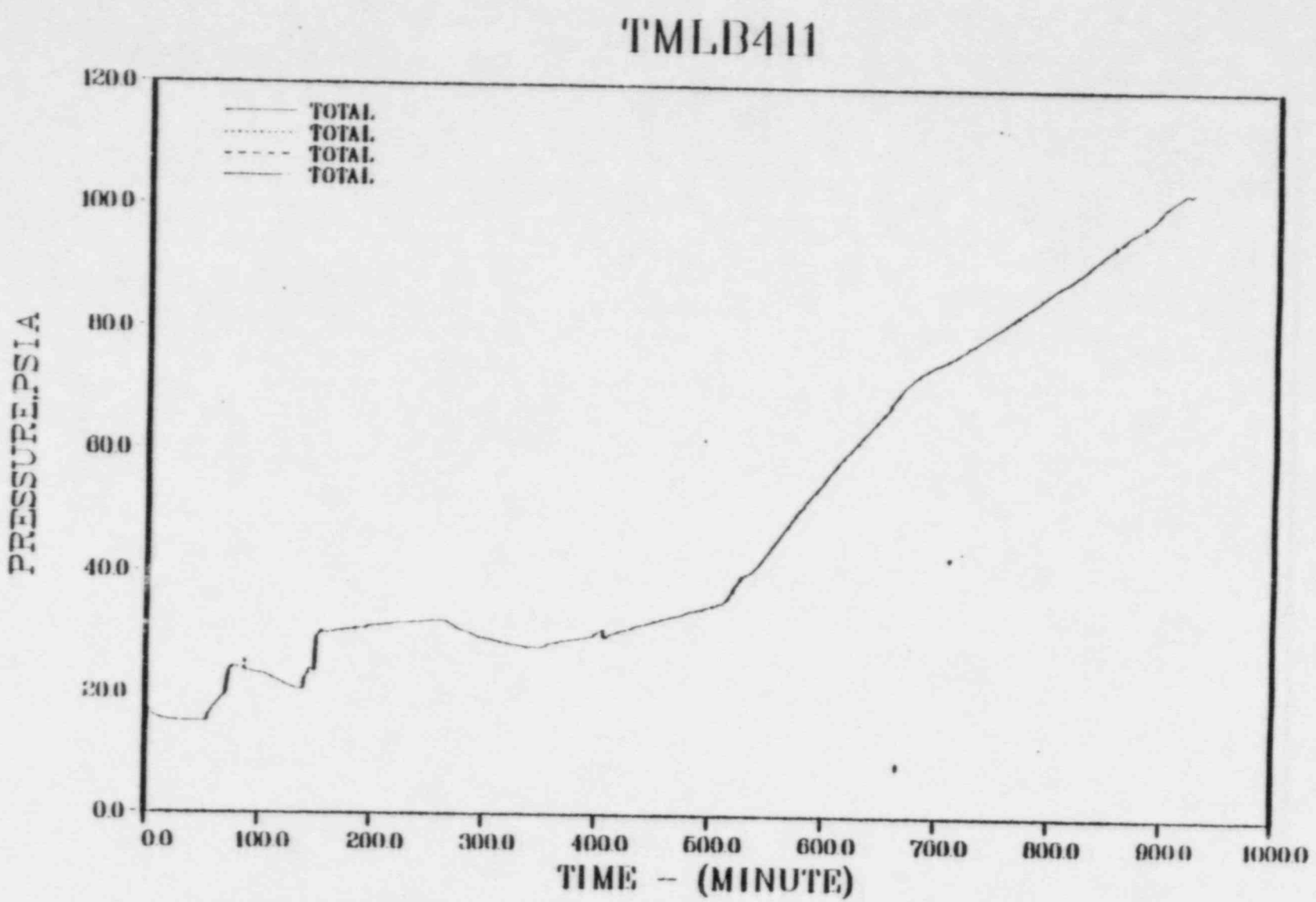

Figure 8

DRAFT

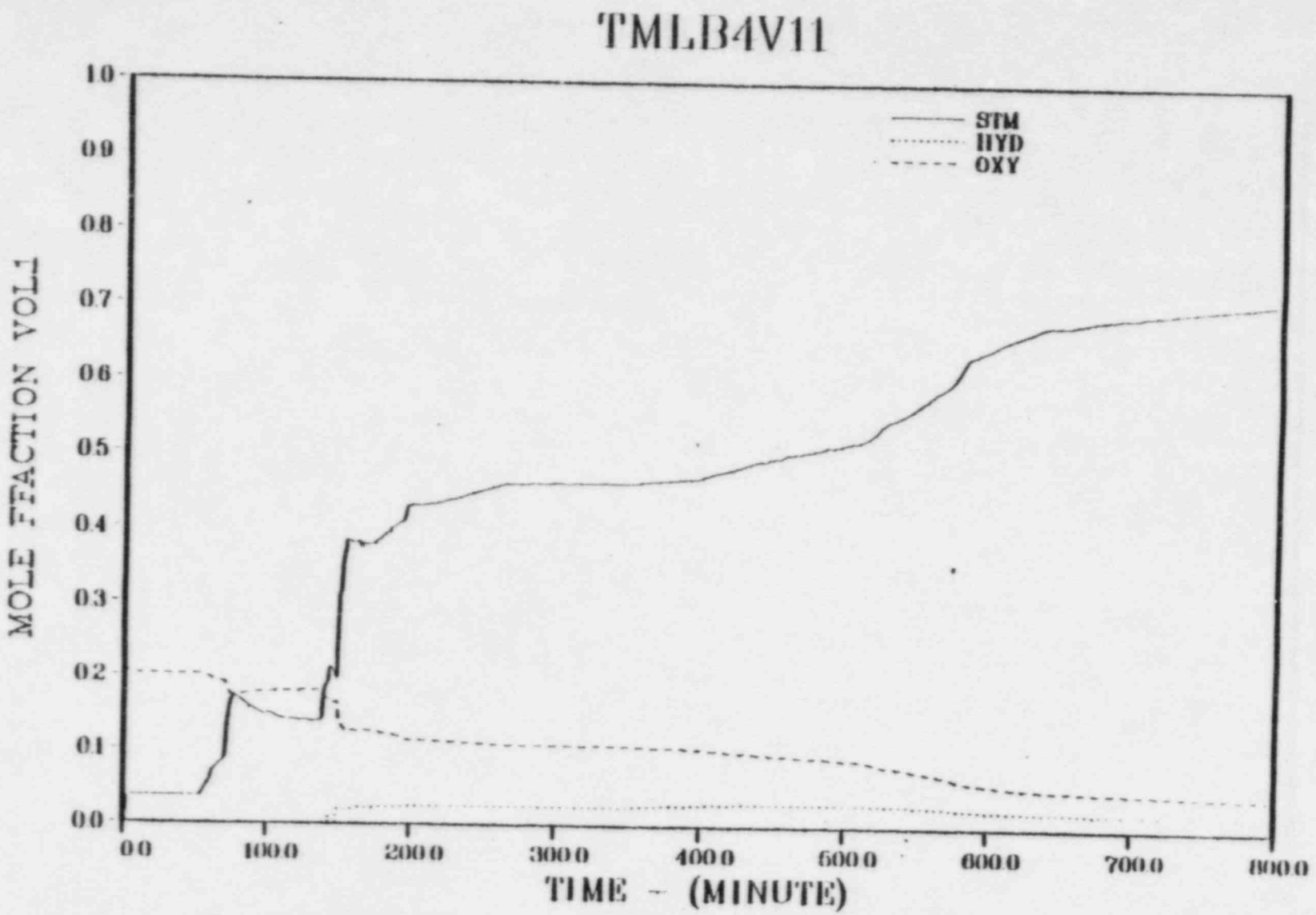
TMLB4V11
STM
HYD
OXY
MOLE FRACTION VOLI
10
09
08
07
06
05
04
03
02
01
00
00
1000
2000
3000
4000
5000
6000
7000
8000
TIME - (MINUTE)

Figure 9

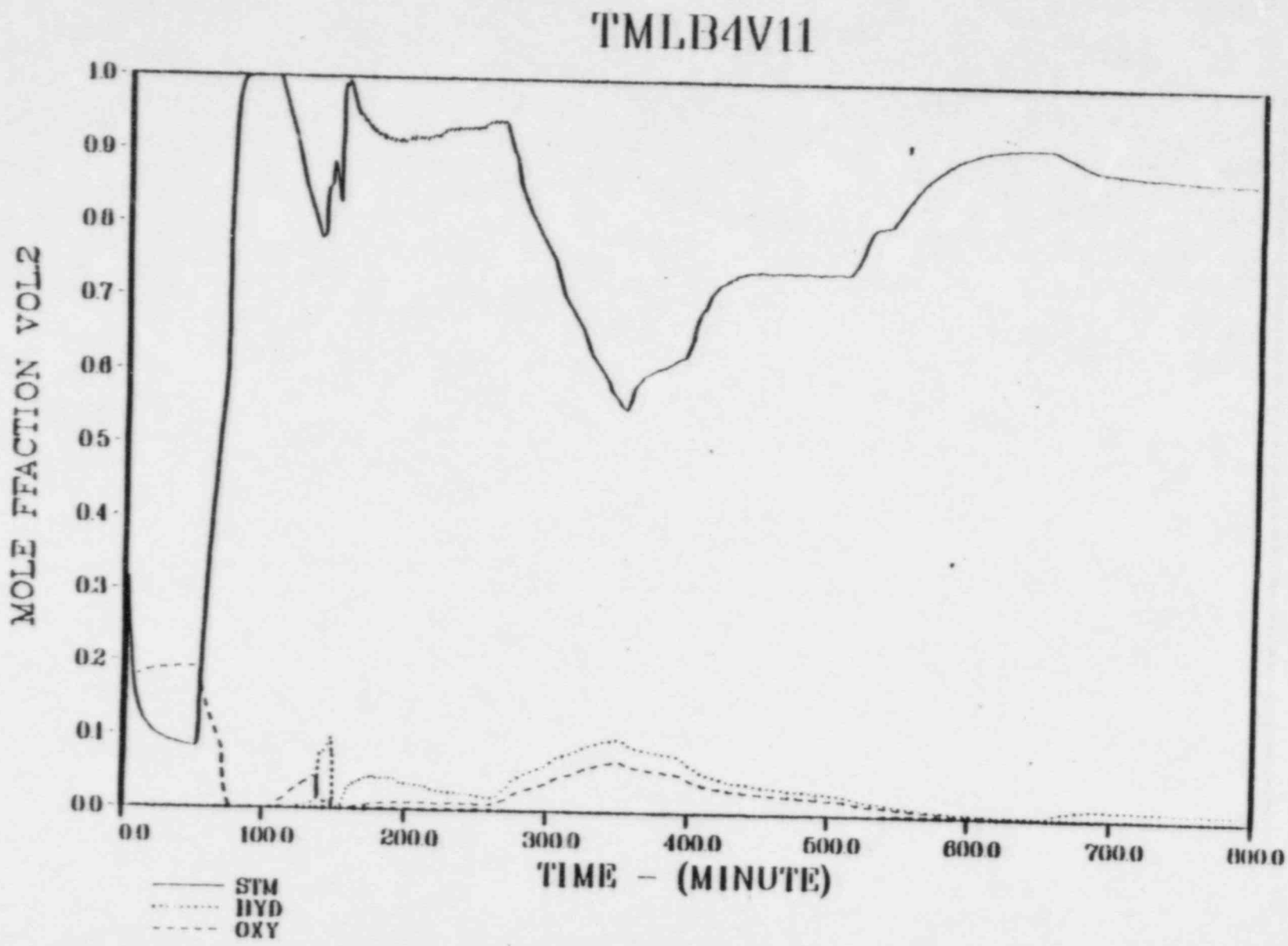
TMLB4V11
MOLE FFACTION VOL2
1.0
0.9
0.8
0.7
0.6
0.5
0.4
0.3
0.2
0.1
0.0
0.0
1000
2000
3000
4000
5000
6000
7000
8000
TIME - (MINUTE)
STM
HYD
OXY

Figure 10

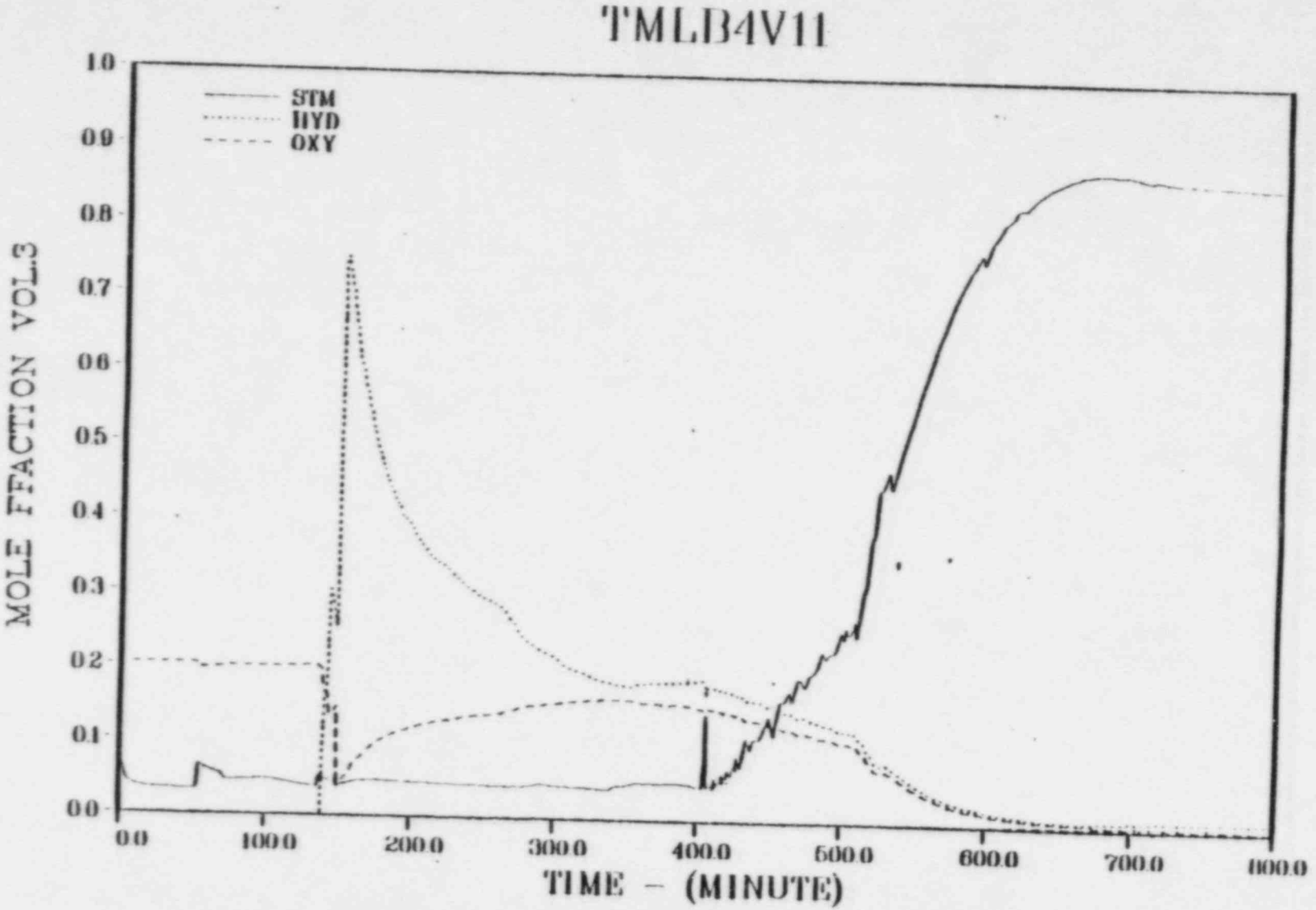
TMLB4V11
STM
HYD
OXY
MOLE FFACTION VOL3
1.0
0.9
0.8
0.7
0.6
0.5
0.4
0.3
0.2
0.1
0.0
0.0
100.0
200.0
300.0
400.0
500.0
600.0
700.0
800.0
TIME – (MINUTE)

Figure 11

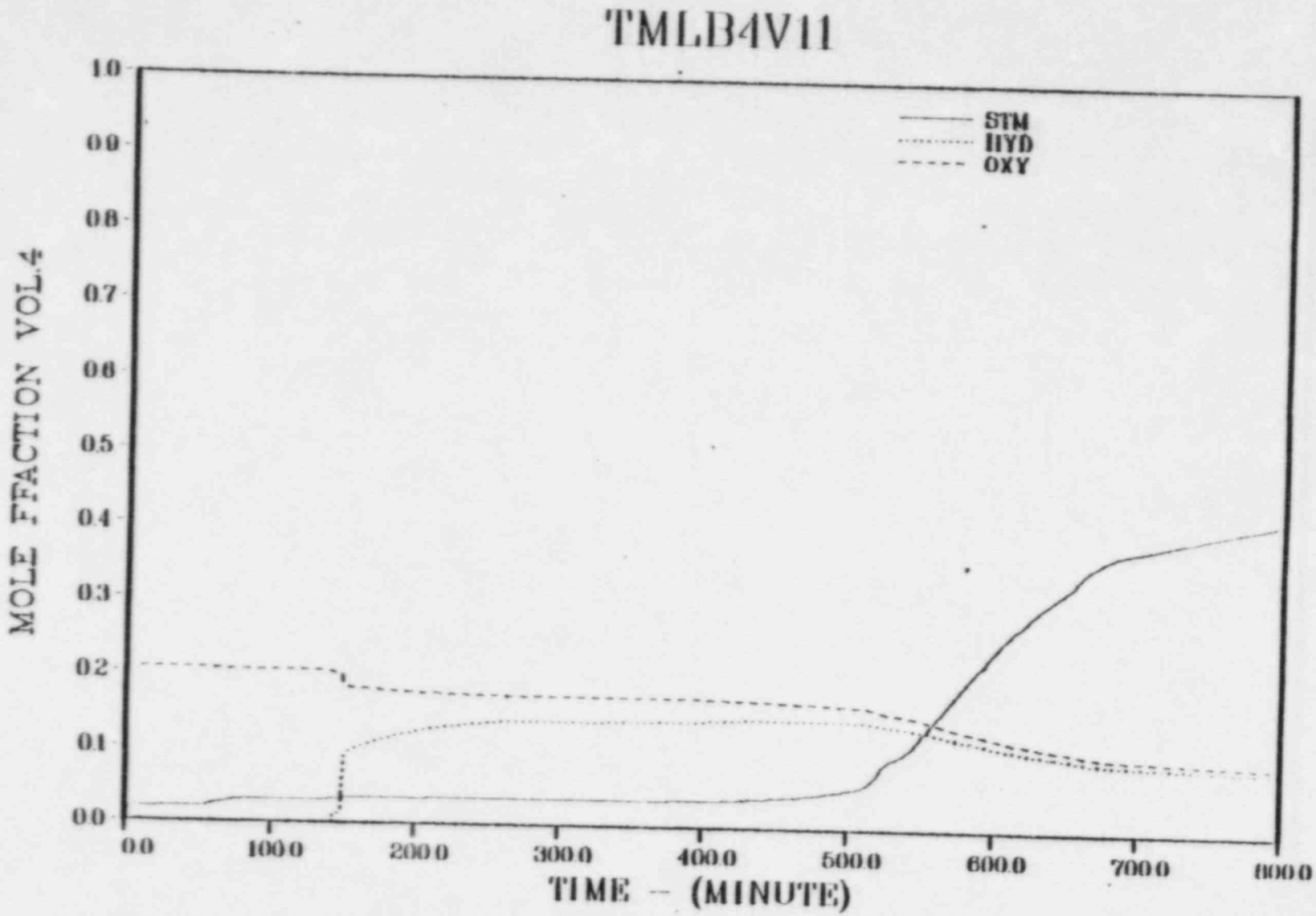

Figure 12

DRAFT

Table II

Table 3. Case Descriptions and Summary of Results

DRAFT

Case No.	In-Vessel Zr Oxid.	Steam Spike	Ignition and Limit	Type (TMI?)	Number of Burns by Compartment 1	2	3	4	5	6	7	8	9	Peak Loadings Pressure, kPa (Comptt.#)	Temperature, K (Comptt.#)	°C	Pressure Dose Pressure, kPa	MPa²
3.00	49.4%	High	VB+2s	4.1	2	2	0	0	1	0	0	1	4	603 (1-3.6-9)	1400 (2)	346	552	4.1
3.00a	49.4%	High	Nonsect.	10.0	1	8	0	0	1	0	0	2	2	667 (all)	1667 (2)	822	206	6.2
3.01	49.4%	High	DI+IC	8.0	1	7	0	0	1	0	1	2	6	729 (1.2)	1422 (2)	729	222	8.0
3.02	49.4%	High	DI all	8.0	1	10	0	0	1	0	1	9	17	574 (all)	1177 (2)	777	302	5.1
3.02a	49.4%	High	Nonsect.	12.0	1	8	0	0	1	0	0	2	4	622 (all)	1762 (2)	1127	220	6.6
3.02a	49.4%	High	Nonsect.	28.0	0	1	0	0	0	0	0	0	1	333 (all)	2042 (2)	422	—	—
3.03	49.4%	High	None	100.0	0	0	0	0	0	0	0	0	0	333 (all)	427 (4)	418	—	—
3.07	49.4%	High	VB	8.0	2	2	0	0	0	0	0	1	1	618 (all)	2138 (2)	476	4aa	4.1
3.08	49.4%	High	VB+5s	8.0	1	2	0	0	0	0	0	1	2	522 (all)	1206 (2)	472	222	4.1
3.09	49.4%	High	VB+10s	8.0	1	2	0	0	0	0	0	2	2	659 (all)	1460 (9)	222	220	8.0
3.10	49.4%	High	VB+20s	8.0	1	2	0	0	0	0	0	1	1	850 (1.2)	1502 (8)	500	296	11.0
3.30	49.4%	Low	VB+2s	8.0	1	2	0	0	0	0	0	1	2	482 (all)	1202 (2)	474	222	4.1
3.31	99.2%	Low	VB+5s	8.0	1	2	0	0	1	0	0	2	2	704 (1.2)	2022 (2)	1077	264	8.7
3.32	99.2%	Low	VB+1hr	8.0	1	1	0	0	1	0	0	1	1	1429 (1.2)	2229 (1)	1819	24a	22.7
3.01	79.4%	High	VB+5s	8.0	2	2	0	0	0	0	0	0	1	602 (1.2)	1446 (2)	470	422	4.1
3.33	79.4%	Low	VB+5s	8.0	1	2	0	0	0	0	0	0	2	467 (all)	1440 (2)	420	224	4.a
V.00	48.2%	High	VB+2s	8.0	0	0	0	0	0	0	0	0	1	1021 (1.2)	1677 (1)	504	248	14.2
V.01	48.2%	High	DI all	8.0	1	8	0	0	0	0	0	2	8	661 (1-3.6-9)	1804 (2)	221	222	8.0

* DI+IC--Deliberate Ignition except in Ice Compartments and Lower Plenum
DI all--Deliberate Ignition in all compartments
VB --Vessel Breach

TABLE III

ICE CONDENSER PWR STANDARD PROBLEM

SUMMARY OF ICE CONDENSER PWR STANDARD PROBLEM RESULTS

In-Vessel Zr Oxide, %	Steam Spike	Ignition Threshold v/o H_2	Ignition Time/Type	Peak Pressure, psia	
				MARCH	HECTR
49	HIGH	NONE	NONE	30	48
49	HIGH	8	DI	76	104
49*	HIGH*	8*	DI*	68*	95*
49	HIGH	8	VB	76	88
49*	HIGH*	8*	VB*	70	150*
49	HIGH	8	VB+5 SEC	77	77
49	HIGH	8	VB+20 SEC	82	122
49	HIGH	10	NON-MECH.	80	95
49	LOW	8	DI	53	
49	LOW	8	VB+5 SEC		70
49	LOW	10	NON-MECH.	48	
100	HIGH	8	VB	135	
100	LOW	8	VB+5 SEC		101
39	HIGH	8	VB+5 SEC		86
39	LOW	8	VB+5 SEC		58
49	HIGH	4.1	VB+5 SEC		86

* EARLY RELEASE OF H_2 FROM PRIMARY.

Table IV

Battelle
Columbus Laboratories